ORNL/TM-2015/489

SCALE Sensitivity and Uncertainty Calculations for the High Flux Isotope Reactor Core Loaded with LEU Fuel

Douglas G. Bowen
Lester M. Petrie, Jr.
Elizabeth L. Jones

Approved for public release.
Distribution is unlimited.

December 20, 2015

OAK RIDGE NATIONAL LABORATORY
MANAGED BY UT-BATTELLE FOR THE US DEPARTMENT OF ENERGY

DOCUMENT AVAILABILITY

Reports produced after January 1, 1996, are generally available free via US Department of Energy (DOE) SciTech Connect.

Website http://www.osti.gov/scitech/

Reports produced before January 1, 1996, may be purchased by members of the public from the following source:

National Technical Information Service
5285 Port Royal Road
Springfield, VA 22161
Telephone 703-605-6000 (1-800-553-6847)
TDD 703-487-4639
Fax 703-605-6900
E-mail info@ntis.gov
Website http://www.ntis.gov/help/ordermethods.aspx

Reports are available to DOE employees, DOE contractors, Energy Technology Data Exchange representatives, and International Nuclear Information System representatives from the following source:

Office of Scientific and Technical Information
PO Box 62
Oak Ridge, TN 37831
Telephone 865-576-8401
Fax 865-576-5728
E-mail reports@osti.gov
Website http://www.osti.gov/contact.html

This report was prepared as an account of work sponsored by an agency of the United States Government. Neither the United States Government nor any agency thereof, nor any of their employees, makes any warranty, express or implied, or assumes any legal liability or responsibility for the accuracy, completeness, or usefulness of any information, apparatus, product, or process disclosed, or represents that its use would not infringe privately owned rights. Reference herein to any specific commercial product, process, or service by trade name, trademark, manufacturer, or otherwise, does not necessarily constitute or imply its endorsement, recommendation, or favoring by the United States Government or any agency thereof. The views and opinions of authors expressed herein do not necessarily state or reflect those of the United States Government or any agency thereof.

ORNL/TM-2015/489

Reactor and Nuclear Systems Division

SCALE SENSITIVITY AND UNCERTAINTY CALCULATIONS FOR THE HIGH FLUX ISOTOPE REACTOR CORE LOADED WITH LEU FUEL

Author(s)

Douglas G. Bowen (ORNL)
Lester M. Petrie, Jr. (ORNL)
Elizabeth L. Jones (University of Tennessee, Knoxville)

Date Published: December 20, 2015

Prepared by
OAK RIDGE NATIONAL LABORATORY
Oak Ridge, Tennessee 37831-6283
managed by
UT-BATTELLE, LLC
for the
U.S. DEPARTMENT OF ENERGY
under contract DE-AC05-00OR22725

CONTENTS

LIST OF FIGURES v
LIST OF TABLES vii
ACKNOWLEDGEMENTS ix
ACRONYMS xi
ABSTRACT xiii
1. INTRODUCTION 1
2. BACKGROUND 3
2.1 HFIR DESCRIPTION 3
2.2 HFIR LEU CORE CONVERSION 6
3. CALCULATION METHODOLOGY 9
3.1 TSUNAMI-3D AND TSUNAMI-IP ANALYSIS USING CONTINUOUS ENERGY CROSS SECTIONS 9
3.1.1 Background 9
3.1.2 TSUNAMI-3D Overview 9
3.1.3 Continuous Energy TSUNAMI-3D Calculations 10
4. CALCULATIONS AND RESULTS 11
4.1 HFIR LEU CORE MODEL 11
4.2 TSUNAMI-3D (CE) RESULTS 13
4.3 DIRECT PERTURBATION CALCULATIONS 26
4.4 CE TSUNAMI CALCULATION DISCUSSION 30
5. TSUNAMI-IP CALCULATIONS 33
5.1 INTERNATIONAL HANDBOOK OF EVALUATED CRITICALITY SAFETY BENCHMARK EXPERIMENTS 33
5.2 SIMILARITY ASSESSMENT 33
5.3 TSUNAMI-IP RESULTS 34
6. TSUNAMI-3D ANALYSIS OF FUEL ELEMENT MODELING ASSUMPTIONS 37
6.1 HOMOGENIZED FUEL ELEMENT ASSUMPTIONS 37
6.2 HOMOGENEOUS AND SLAB TSUNAMI-3D CALCULATIONS 37
6.2.1 Description of the Homogeneous and Slab TSUNAMI-3D Models 37
6.2.2 Homogeneous and Slab Model Results 39
7. CONCLUSION 52
REFERENCES 54

LIST OF FIGURES

Figure **Page**

Fig. 1. A vertical section of the HFIR core and vessel [10].....4
Fig. 2. HFIR fuel design [10].....5
Fig. 3. Top view of a HFIR fuel bundle [11].....6
Fig. 4. Cross section of the CE TSUNAMI-3D model for HFIR LEU core.....11
Fig. 5. Axial cross section of the TSUNAMI-3D model for HFIR LEU core.....12
Fig. 6. HFIR LEU core and flux trap region in the LEU Core model. 12
Fig. 7. Energy-dependent sensitivity profiles for ^{1}H (capture, elastic scatter, and total). 14
Fig. 8. Energy-dependent sensitivity profiles for ^{9}Be (capture, elastic scatter, and total).....15
Fig. 9. Energy-dependent sensitivity profile for 9Be(n,2n). 16
Fig. 10. Neutron cross section for ^{9}Be(n,2n) reaction.....17
Fig. 11. Energy-dependent sensitivity profiles for ^{235}U (capture, elastic scatter, total, and fission). 18
Fig. 12. Energy-dependent sensitivity profile for ^{235}U inelastic scattering (n,n'). 19
Fig. 13. Energy-dependent sensitivity profiles for ^{238}U (capture, elastic scatter, total, and fission). 20
Fig. 14. Energy-dependent sensitivity profile for ^{238}U inelastic scattering (n,n'). 21
Fig. 15. Energy-dependent sensitivity profiles for various molybdenum isotopes (elastic scatter). 22
Fig. 16. Energy-dependent sensitivity profiles for ^{95}Mo (elastic scattering). 23
Fig. 17. Energy-dependent sensitivity profiles for various molybdenum isotopes (inelastic scattering).....24
Fig. 18 Energy-dependent sensitivity profiles for various molybdenum isotopes (capture). 25
Fig. 19. Energy-dependent sensitivity profiles for ^{95}Mo (capture). 26
Fig. 20. Graphical DP results for ^{9}Be bound. 28
Fig. 21. Graphical DP results for ^{1}H. 28
Fig. 22. Graphical DP results for Mo.....29
Fig. 23. Graphical DP results for ^{235}U. 29
Fig. 24. DP Graphical results for ^{238}U. 30
Fig. 25. Composite plot of TSUNAMI-IP comparison results for the HFIR LEU core model.....35
Fig. 26. TSUNAMI-IP comparison results with highest similarity index. 35
Fig. 27. Energy-dependent sensitivity profiles for ^{235}U (total) for the slab and homogeneous LEU fuel plate configurations. 42
Fig. 28. Energy-dependent sensitivity profiles for ^{235}U (fission and capture) for the slab and homogeneous LEU fuel plate configurations. 43
Fig. 29. Energy-dependent sensitivity profiles for ^{238}U (Total) for the slab and homogeneous LEU fuel plate configurations.....44
Fig. 30. Energy-dependent sensitivity profiles for ^{238}U (fission and capture) for the slab and homogeneous LEU fuel plate configurations. 45
Fig. 31. Energy-dependent sensitivity profile for ^{235}U and ^{238}U (elastic scattering) for the slab and homogeneous LEU fuel plate configurations. 46
Fig. 32. Energy-dependent sensitivity profile for ^{1}H (Capture) for the slab and homogeneous LEU fuel plate configurations.....47
Fig. 33. Energy-dependent sensitivity profile for ^{1}H (elastic scattering) for the slab and homogeneous LEU fuel plate configurations. 48
Fig. 34. Energy-dependent sensitivity profile for ^{95}Mo, ^{96}Mo, and ^{98}Mo (capture) for the slab and homogeneous LEU fuel plate configurations. 49
Fig. 35. Energy-dependent sensitivity profile for ^{95}Mo, ^{96}Mo, and ^{98}Mo (elastic scattering) for the slab and homogeneous LEU fuel plate configurations. 50

LIST OF TABLES

Table **Page**

Table 1. Energy-integrated sensitivities and standard deviations for HFIR loaded with LEU fuel 13
Table 2. Comparison of CE TSUNAMI and direct perturbation results 27
Table 3. Similarity index values for benchmark-critical experiments from TSUNAMI-IP analysis 36
Table 4. Slab model material specifications 38
Table 5. Homogeneous model material specifications 39
Table 6. Comparison of CE TSUNAMI and DP results for the homogeneous configuration.....40
Table 7. Comparison of CE TSUNAMI and DP results for the explicit slab configuration 40
Table 8. Comparison of CE TSUNAMI results for homogeneous and slab configurations.....41
Table 9. Energy-integrated sensitivities and standard deviations for the homogeneous and explicit slab configuration 41

ACKNOWLEDGEMENTS

The authors wish to acknowledge Chris Perfetti and Brad Rearden for developing the continuous energy TSUNAMI-3D methodologies that allowed this work to be possible. They also reviewed the preliminary results for this work to ensure the preliminary code package was functioning as intended. Their scrutiny of the preliminary results and suggestions for improving them greatly contributed to quality of this work. The authors also wish to acknowledge those on the SCALE team who worked with the authors of this report to solidify the continuous energy TSUNAMI-3D capabilities of SCALE in time to support this work. The authors are also grateful for support, information, and reviews provided by David Renfro, David Cook, and technical reviews by Don Mueller and Germina Ilas.

ACRONYMS

CE	continuous energy
CLUTCH	Contribution-Linked Eigenvalue Sensitivity/Uncertainty Estimation via Tracklength Importance Characterization
DOE	US Department of Energy
DP	direct perturbation
ENDF	evaluated nuclear data file
HEU	highly enriched uranium
HFIR	High Flux Isotope Reactor
IEU	intermediate enriched uranium
IFE	inner fuel element
IFP	Iterated Fission Probability (methodology)
IHECSBE	*International Handbook of Evaluated Criticality Safety Benchmark Experiments*
LEU	low enriched uranium
LPCF	low power critical facility
MB	megabyte
MCNP	Monte Carlo N-Particle
MW	megawatt
NNSA	National Nuclear Security Administration
NRAD	National Radiography (Reactor)
OFE	outer fuel element
ORNL	Oak Ridge National Laboratory
RERTR	Reduced Enrichment for Research and Test Reactor (Program)
TSUNAMI	Tools for Sensitivity and Uncertainty Analysis Methodology

ABSTRACT

The objective of this work is to perform sensitivity/uncertainty (S/U) analyses to investigate the quantitative need for benchmark-quality integral experiments for the validation of computational methods used to support the conversion of the High Flux Isotope Reactor (HFIR) from Highly Enriched Uranium (HEU) to Low Enriched Uranium (LEU) fuel. This report presents the results of a series of HFIR LEU fuel calculations performed with the TSUNAMI-3D code package. The TSUNAMI-3D code in the SCALE nuclear analysis code system generates k_{eff} sensitivity coefficients for criticality safety and reactor physics applications. These coefficients can be used to quantify the computational bias and bias uncertainty of the analyzed system in the absence of directly applicable benchmark-quality critical experiments. This report presents results for a LEU HFIR model that were generated with TSUNAMI-3D using the new CLUTCH methodology and continuous-energy (CE) cross sections. The CE TSUNAMI-3D sequence was used to determine nuclide cross section sensitivities and uncertainties that can affect the k_{eff} for the analyzed HFIR LEU core model.

The results of the sensitivity/uncertainty analysis show that the largest sensitivities of k_{eff} occur with ^{1}H elastic scattering, ^{235}U fission, and ^{235}U capture cross sections, with CE TSUNAMI-computed integral sensitivities of about 0.27, -0.16, and 0.30, respectively. The system k_{eff} is modestly sensitive to small changes in ^{9}Be elastic scattering cross-section (~0.04), which is expected as HFIR has a large beryllium reflector surrounding the core. The HFIR LEU core fuel contains 90 wt. % uranium and 10 wt. % natural molybdenum, and the k_{eff} appears to be sensitive to small perturbations in molybdenum capture reactions, although the total integral capture sensitivity for all molybdenum isotopes is on the order of 10^{-2}. There is less sensitivity to ^{238}U nuclear data perturbations than were expected considering that the ^{238}U concentration increases significantly with the HFIR core fuel modification from highly enriched uranium (HEU) (~93.2 wt. % ^{235}U) to LEU (~19.75 wt. % ^{235}U) fuel. The integral sensitivity for ^{238}U capture reactions is about -0.08. The direct perturbation (DP) calculations compared well with the CE TSUNAMI-3D results overall. Multigroup TSUNAMI-3D could not be successfully applied to the complex HFIR LEU model. The new CE TSUNAMI-3D sequence of SCALE has made it possible to perform sensitivity analyses for complex geometrical configurations such as the HFIR LEU core.

The TSUNAMI-IP utility was also used to determine applicable benchmark critical experiments for validation efforts. The c_k values generated by TSUNAMI-IP serve as an index for similarity assessment and represent the correlation of k_{eff} uncertainties between two models. This index quantifies the amount of shared uncertainty in the k_{eff} values of an application and a benchmark critical experiment due to uncertainties in the cross sections. A c_k value of 1.0 indicates that the uncertainties for the model and the critical benchmark experiment are from the same neutron cross sections, and their reactions at the same energy, while a c_k value of 0.0 indicates that the uncertainties are completely unrelated. Typically, a c_k value of 0.9 or larger indicates good shared uncertainty between the model and the benchmark experiment. The results from this work show that none of the nearly 750 critical benchmark experiments examined had a c_k index greater than 0.9;there were 112 experiments that had a c_k value between 0.8 and 0.9, indicating some moderate similarity with the HFIR LEU core model. One conclusion that can be drawn from this comparison analysis is the need for benchmark-quality critical experiments for an LEU HFIR core to support criticality safety and reactor physics calculations for core conversion activities. It would be desirable for these measurements to be performed in a facility such as the proposed LPCF at ORNL. The close proximity to the HFIR reactor facility would allow measurements of excess reactivity to be performed to verify manufacturing techniques in a manner similar fashion to those performed by the Y-12 critical experiment facility in the 1960s prior to the new cores being loaded into the pressure vessel.

Simple homogeneous (mixture of fuel, clad, and moderator) and heterogeneous slab (flat fuel plate) representations of HFIR fuel plates in CE TSUNAMI-3D were generated to explore the effects of

different geometric approximations.. A homogeneous arrangement of fuel, clad and moderator could increase resonance self-shielding in the fuel. This is indicated with a larger k_∞ result for the heterogeneous configuration compared to that for the homogeneous configuration. In general, the results of these calculations show larger k_{eff} integral sensitivities to small cross section changes in molybdenum isotopes, ^{235}U, and ^{238}U for the homogeneous rather than for the heterogeneous fuel plate configuration, with differences of 4.07%, 8.70%, and 6.66%, respectively. The exception was ^{1}H, which had a total integral sensitivity which was 10.95% larger for the explicit slab configuration than for the homogeneous configuration.

Future work may involve (1) using the HFIR LEU model with the IFP methodology available in CE TSUNAMI-3D, (2) using the HFIR HEU model to compare to HFIR LEU model CE TSUNAMI-3D results presented here, and (3) performing S/U calculations using the Whisper methodology in MCNP to compare to the results of the CE TSUNAMI-3D results in this report.

1. INTRODUCTION

The Oak Ridge National Laboratory (ORNL) is investigating the feasibility of converting the High Flux Isotope Reactor (HFIR) from highly enriched uranium (HEU) fuel to low-enriched uranium (LEU) fuel. These efforts are performed as part of an effort sponsored by the US Department of Energy (DOE) National Nuclear Security Administration (NNSA). These efforts include engineering design studies for the core conversion using a variety of computational models that consider proposed HFIR LEU fuel designs to determine if an LEU core can meet the conversion requirements and maintain reactor performance parameters similar to those of the HEU core. Studies performed to date have demonstrated that the current HFIR core performance can be maintained with an LEU core with respect to the neutron flux in the central target region, reflector, and beam tube locations assuming that the core power increases from 85 MW to 100 MW [1]. The studies used nuclear data libraries (cross-section data) that are based on the Evaluated Nuclear Data Files (ENDF). Biases and uncertainties associated with modeling simplifications and the use of these nuclear data libraries can affect the results of the complex radiation transport calculations. Results that can be affected include preliminary reactor physics and engineering design studies for the HFIR LEU core conversion. The objective of this work is to perform sensitivity/uncertainty (S/U) analyses to investigate the quantitative need for benchmark-quality integral experiments to support the validation of computational methods used to support the conversion of the HFIR from HEU to LEU fuel. This report presents the results of a series of HFIR LEU fuel calculations performed with the SCALE [2] code TSUNAMI-3D.

The TSUNAMI-3D [3] code package generates k_{eff} sensitivity* coefficients for criticality safety and reactor physics applications. These coefficients can be used to quantify the computational bias and bias uncertainty of the analyzed system in the absence of directly applicable benchmark-quality critical experiments. The sensitivity coefficients calculated by TSUNAMI-3D describe the fractional change in the system response as a result of small changes to system parameters and cross-section data [4]. The sensitivity coefficients can also be used to assess the neutronic similarity between different critical systems.

When the HFIR HEU cores were designed in the 1960s, critical experiments were performed at Y-12 to provide data used in design efforts and to verify that the HEU cores met manufacturing specifications prior to their use. The capability to perform critical experiments to assist with LEU core design efforts is no longer available at Y-12.

Based on a HFIR HEU core model [5] developed with the SCALE Monte Carlo code KENO VI [6], a HFIR LEU core model was created as a first step in developing a TSUNAMI-3D model using multigroup cross sections. The multigroup TSUNAMI-3D computations failed to execute properly due to the limited computing capabilities available at the time. The complex HFIR LEU core model was then simplified significantly to reduce the computing resources necessary, but the sensitivity coefficient results were poor, so calculations were not pursued further. The need to model complex problems with increased accuracy motivated the development of a new version of TSUNAMI-3D utilizing continuous-energy (CE) cross sections (CE TSUNAMI-3D) instead of multigroup cross sections. The current multigroup version of TSUNAMI-3D calculates sensitivity coefficients by running forward and adjoint KENO calculations to tally forward and adjoint fluxes as a function of space, energy, and angle on a given spatial mesh. The multigroup forward and adjoint fluxes are then used in a linear perturbation theory method described in Ref. 3 to generate the sensitivity coefficients. This multigroup methodology can present challenges with respect to producing accurate sensitivity coefficient results for complex problems due to an inadequately resolved spatial mesh [4] and approximations necessary to generate implicit sensitivities. The CE

* Discussions about sensitivity data in this report refer to only k_{eff} sensitivities.

TSUNAMI-3D code includes two new methods to calculate sensitivity coefficients: (1) the Iterated Fission Probability (IFP) method and (2) the Contribution-Linked Eigenvalue Sensitivity/Uncertainty Estimation via Track-length Importance Characterization (CLUTCH) method. These two methods perform well for calculating eigenvalue sensitivity coefficients in CE Monte Carlo [4]. The CLUTCH methodology was chosen for this work. As shown in this report, CE TSUNAMI-3D produced good results based on a comparison of the TSUNAMI-3D results and direct perturbation calculations.

The S/U analysis for the HFIR LEU core model determines those nuclide cross sections (indicated by larger k_{eff} uncertainties) that are most likely to result in biases affecting the calculated system k_{eff}. In addition, the S/U analysis techniques may be used to identify applicable benchmark critical experiments for use with HFIR LEU core validation efforts and in the design of subcritical or critical experiments that could be performed in an LPCF. HFIR LEU critical experiments in an LPCF would be used to validate the HFIR LEU core conversion computational methodologies and to provide directly applicable benchmark critical experiments for validation purposes, in addition to supporting other core conversion and core design efforts.

Currently, HFIR LEU and HEU reactor physics studies are performed using high-fidelity core models with an explicit representation of the involute-shaped fuel plates [7, 8]. However, all previous HFIR models have approximated the HFIR inner and outer fuel elements by homogenizing the fuel, clad, and moderator and organizing the core materials into radial and axial segments because of difficulties at the time in explicit modeling of the involute geometry of the HFIR fuel plates. To examine the effect of these HFIR fuel element approximations, explicit versus homogenized, on the resonance self-shielding calculations, two additional CE TSUNAMI-3D calculations were performed in this work. These calculations would determine the differences between the sensitivity coefficients for an infinite homogeneous mixture of HFIR LEU fuel, clad, and moderator and an infinite lattice of slab LEU fuel plates in a water moderator that were modeled based on actual fuel, cladding, and water channel thicknesses This work includes calculations to examine both the material and geometric self-shielding characteristics for the HFIR LEU inner and outer fuel element representations and their effect on the sensitivity coefficients. Recent modeling and simulation efforts for HFIR HEU and LEU cores [7, 8] that explicitly modeled the HFIR fuel plate involute geometry and compared the results with those obtained with HFIR homogenized fuel models [1] showed small differences between the eigenvalues and cycle lengths for the HEU core, but significant cycle length differences for the LEU core. Additionally, the desire was to enhance existing models as much as possible as capabilities became available. At this time, it is not possible to explicitly model the involute fuel plates in a CE TSUNAMI-3D model, although the capability will be available in a future version of SCALE. A future version of MCNP contains a sensitivity and uncertainty analysis methodology, called Whisper [9], that uses benchmark critical experiments, nuclear data sensitivities from MCNP, and nuclear covariance data to set a baseline upper subcritical limits, calculated using a non-parametric, extreme-value method.

2. BACKGROUND

2.1 HFIR DESCRIPTION

HFIR is an 85-MW, very high flux pressurized light-water–cooled and –moderated flux-trap reactor [10]. Core heat is dissipated via water circulation through heat exchangers and a cooling tower outside the reactor facility. The HFIR core consists of two concentric fuel annuli (elements) that are currently fueled with HEU fuel (93.2 wt. % enriched ^{235}U) The center of the fuel annuli contains a flux trap region for irradiating targets. The HFIR core is surrounded by a thin water region, a region containing two control elements, and a beryllium reflector region that contains experimental facilities and four beam tubes for use with neutron scattering experiments. Each control element contains three longitudinal regions clad in aluminum: a black region containing europium, a gray region containing tantalum, and a white region containing aluminum [10]. The HFIR pressure vessel resides in a large pool of water adjacent to a spent fuel staging area. The HFIR fuel elements consist of a series of fuel plates with an involute geometry. The HFIR inner fuel element currently has 171 fuel plates with a total ^{235}U loading of about 2.6 kg. The HFIR outer fuel element has 369 fuel plates with a total ^{235}U loading of approximately 6.8 kg. The cycle length of HFIR with HEU fuel varies between 24 and 26 days. HFIR's missions are to support neutron scattering experiments, isotope production, and materials irradiation research. Fig. 1 shows a vertical section of the HFIR vessel and core, in addition to experimental and cooling support equipment [10]. Fig. 2 and Fig. 3 illustrate the HFIR HEU inner and outer fuel elements and show the involute geometry of the fuel plates.

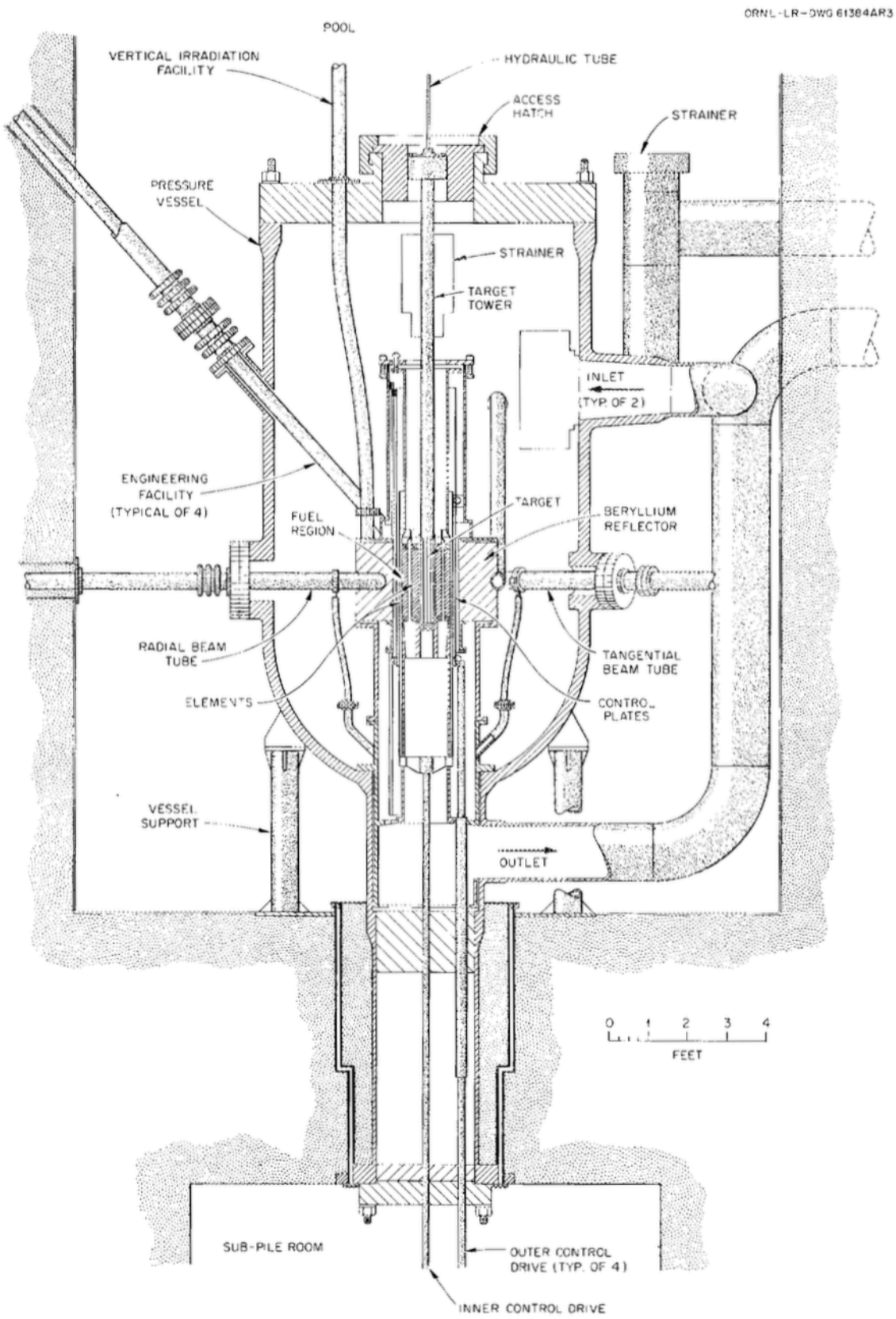

Fig. 1. A vertical section of the HFIR core and vessel [10].

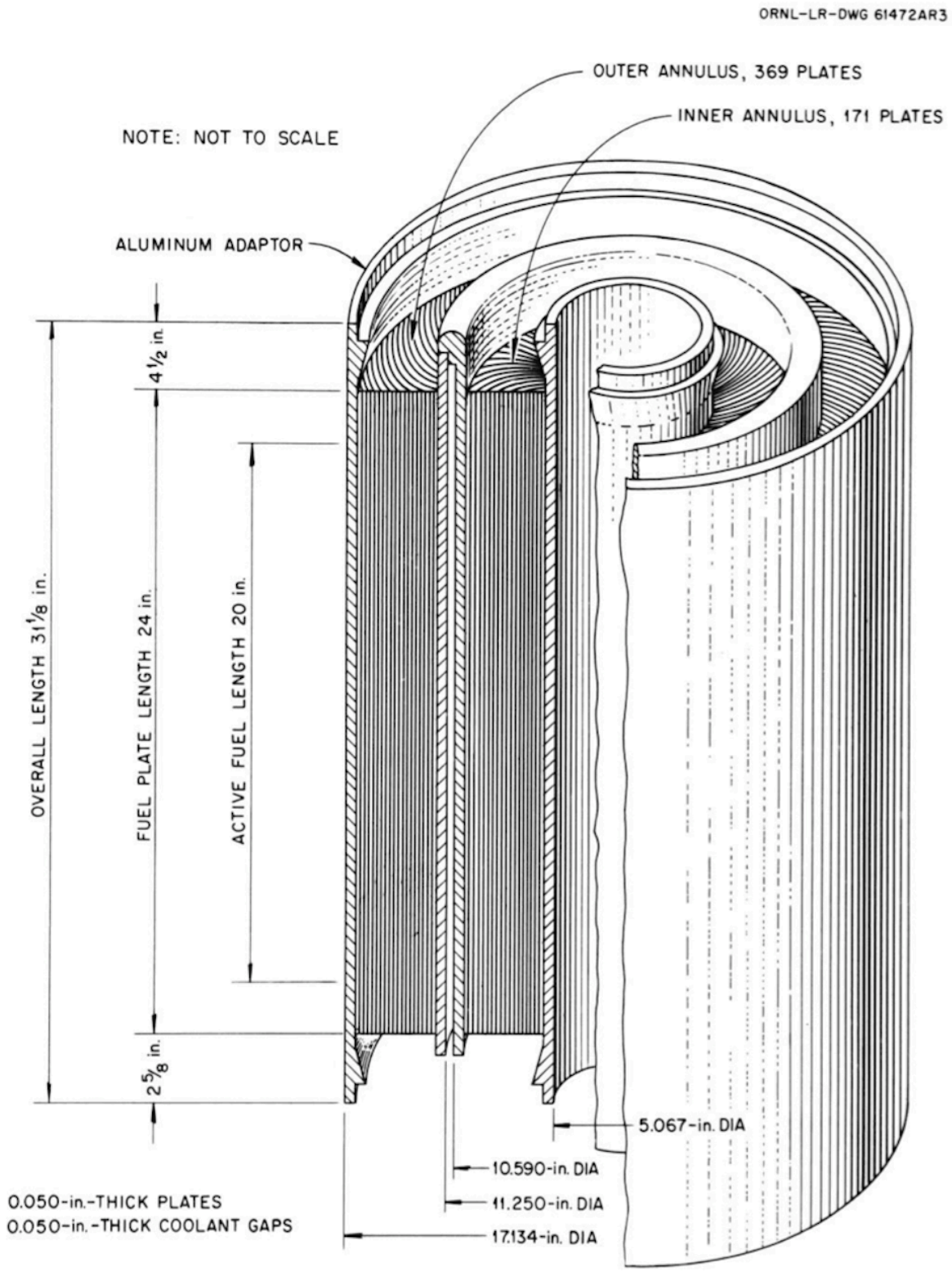

Fig. 2. HFIR fuel design [10].

Fig. 3. Top view of a HFIR fuel bundle [11].

2.2 HFIR LEU CORE CONVERSION

The NNSA LEU conversion effort was established to minimize and, to the extent possible, eliminate the use of HEU in civilian nuclear applications by working to convert research and test reactors and radioisotope production processes to the use of LEU fuel and targets throughout the world [11]. This effort has initiated and supported various studies at a number of US reactor facilities related to fuel development and engineering studies to convert the US high-performance research reactors from HEU fuel to LEU fuel.

Although the HFIR HEU core and the proposed HFIR LEU cores are inherently different (e.g., enrichment, fuel design, and LEU monolithic vs. HEU dispersion form fuel), the overall performance of a HFIR LEU core is required to be the same as the current HFIR HEU core. The following core parameters must be maintained and are assumed to remain the same for the core conversion studies. These assumptions are summarized below [11].

- The HFIR LEU core should have flux levels similar to the HEU core at key locations and cycle length.
- The core dimensions should remain the same.

- There should be no change in the involute fuel plate geometry and minimum clad thickness when using physical dimensions similar to those in the HEU core.
- Based on computational studies, the fuel contouring within individual plates is likely to change to optimize the core power distribution and maintain a radially flat power distribution.
- Margins of safety as discussed in the bases for the technical safety requirements shall be maintained.
- No change will be made in core coolant flow requirements or primary coolant system pressure.
- Each fresh LEU inner fuel element (IFE) and outer fuel element (OFE) shall be separately subcritical under all normal and credible abnormal conditions with conservative reflector conditions (concrete/full water).
- No change will be made to the currently approved methods for handling and storing irradiated fuel elements.

The HFIR LEU studies documented to date [1, 12] examined key parameters for LEU fuel, including fuel and flux trap void coefficients of reactivity, coolant temperature coefficient of reactivity, effect of fuel grading, and thermal hydraulics behavior. These studies have shown that the more dense LEU fuel will provide similar performance as the HEU fuel. Favorable results presented in these studies imply minimal impact to overall HFIR mission performance; however, experimental measurements are highly desirable to validate results of HFIR core computations to ensure confidence in the nuclear data and computational methodology. Efforts to convert other research reactor facilities, such as the Neutron Radiography (NRAD) Reactor at Idaho National Laboratory [13], have resulted in issues related to accurately predicting excess core reactivity with the computational techniques used at the time. Critical experiments could have prevented some of the issues, because if experimental data had been available, it could have been used to verify and validate design calculations.

When the HFIR HEU core was designed, four sets of critical experiments were performed at the Y-12 critical experiment facility [10]. These experiments were used to compile experimental data for a variety of key operational parameters for HFIR: power distribution, moderator-poison data, symmetrical control element positions in the clean core, shutdown margins, control element differential worth, worth of target and voids in the flux trap region, temperature coefficients, neutron lifetime, and effective delayed neutron fraction [10]. Even after the production HFIR HEU cores started to arrive at ORNL, the Oak Ridge Critical Experiment Facility at the Y-12 National Security Complex performed critical measurements on the new cores to verify the fuel elements prior to their use in the HFIR pressure vessel. The ability to perform critical experiments with proposed HFIR LEU conversion activities to verify that the LEU cores are manufactured to specifications before being loaded into the reactor vessel would be invaluable to verify reactor physics computations and to develop experimental benchmarks to validate computer codes and nuclear data. The DOE currently does not have the capability to perform HFIR critical experiments.

3. CALCULATION METHODOLOGY

3.1 TSUNAMI-3D AND TSUNAMI-IP ANALYSIS USING CONTINUOUS ENERGY CROSS SECTIONS

3.1.1 Background

A KENO-VI model of an LEU HFIR core was developed for preliminary studies related to this work to perform preliminary sensitivity/uncertainty (S/U) analyses with the multigroup version of TSUNAMI-3D and to calculate the system effective multiplication factor, k_{eff}. The "multi-region" option was used in the TSUNAMI-3D sequence to account for both geometric and material resonance self-shielding effects in the calculations. These calculations utilized the 238-group cross sections set derived from ENDF/B-VII data. This calculation did not succeed due to computer memory limitations. The version of the SCALE code system currently under development includes a new version of the TSUNAMI-3D package that uses CE cross sections [4]. The use of CE cross sections eliminates the need to perform rigorous resonance self-shielding calculations to generate a case-dependent multigroup cross section library for use with the HFIR LEU multigroup core model. Future work should consider using Whisper [9] to allow for MCNP S/U analyses to be performed to compare to the CE TSUNAMI-3D results.

3.1.2 TSUNAMI-3D Overview

Tools for Sensitivity and Uncertainty Analysis Methodology Implementation in Three Dimensions (TSUNAMI-3D) is a SCALE control module that facilitates the application of sensitivity and uncertainty analysis to criticality safety analysis using the first-order linear perturbation method. TSUNAMI-3D provides for the automated processing of the HFIR LEU core model materials, the processing of multigroup cross sections (including the self-shielded, case-dependent, cross section data for this particular problem), the calculation of forward and adjoint neutron transport solutions, the calculation of the k_{eff} sensitivity coefficients, and the calculation of the uncertainty in k_{eff} due to the cross section covariance (uncertainty) data. The SAMS module is used to determine the sensitivity of the calculated value of k_{eff} to the nuclear cross-section data used in the calculation as a function of material, reaction type, and neutron energy. The sensitivity data file produced by TSUNAMI-3D is then processed through a SCALE module, TSUNAMI-IP (Tools for Sensitivity and Uncertainty Analysis Methodology Implementation – Indices and Parameters), to determine the degree of similarity between two systems [14]. Specifically, an index used for a comparison or similarity assessment is the correlation of uncertainties in the k_{eff} for a system (c_k). This index is used to quantify the amount of shared uncertainty in the k_{eff} values between the HFIR LEU core and a benchmark critical experiment based on uncertainties in the nuclear cross sections. Therefore, a c_k value of 1.0 means that the uncertainties for the application and the benchmark are all generated from the same nuclides and reactions at the same energies, whereas a c_k value of 0.0 means that the uncertainties of the two systems are completely unrelated [14]. If the HFIR LEU model and a critical experiment have the same energy-dependent sensitivities to the same nuclear data, they should have the same computational bias. Use of the c_k correlation coefficient ensures that the nuclear data resulting in the higher k_{eff} uncertainties receive greater weight when model sensitivities are compared. This analysis will allow a comparison of the HFIR LEU core model and the potential benchmark-critical experiments for use in validation and verification efforts. Applicable similarity between the HFIR LEU model results and a critical benchmark experiment is indicated if the calculated c_k value is greater than 0.9 and less than 0.95, and high applicability is indicated if the calculated c_k value is greater than 0.95 [15].

3.1.3 Continuous Energy TSUNAMI-3D Calculations

ORNL has developed new capabilities allowing CE eigenvalue sensitivity coefficient calculations with TSUNAMI-3D [4, 16]. These new capabilities will be included in SCALE 6.2, the next release of the SCALE package (anticipated release in FY2016). This capability was developed because many TSUNAMI-3D end users needed to model more complex problems with increased accuracy. As previously discussed, the HFIR LEU TSUNAMI-3D multigroup model produced inaccurate results due largely to an inadequately resolved spatial mesh in the transport calculations and computer memory limitations, as the multigroup cross sections were being adjusted for resonance self-shielding effects. Two additional methods in the CE TSUNAMI-3D code have been developed to enhance the capabilities of TSUNAMI-3D. These methods use CE cross sections: the Integrated Fission Probability (IFP) method and the Contribution-Linked eigenvalue sensitivity/Uncertainty estimation via track length importance Characterization (CLUTCH) method. The IFP and CLUTCH methods are thoroughly discussed in Reference 16. These methods have been implemented within the Monte-Carlo KENO code in SCALE, which has the capability to use CE cross sections. The new methods calculate the eigenvalue sensitivity coefficients during a single forward Monte-Carlo calculation without the use of a spatial mesh to avoid a significant limitation of the multigroup TSUNAMI-3D approach [16].

According to the summary in Reference 16, the IFP method computes adjoint-weighted tallies using the concept that the importance of an event (relative to the k_{eff} of the system) is proportional to the population of neutrons present in the system that are progeny of the original event. In a practical sense, this method requires storing reaction rate tallies for simulated particles in the calculation for some number of generations until the population of their progeny has reached an asymptotic value-to-weight reaction rate tallies for the original neutron to subsequently produce sensitivity coefficient estimates via the first-order perturbation equation [16]. This method requires a great deal of execution time, depending on the problem's complexity. For this reason, the IFP method was not used for this analysis. The CLUTCH method calculates the importance of events during a particle's lifetime by examining how many fission neutrons are created by that particle after those events occur. This method requires that reaction rate information be stored by the calculation for every interaction event in the particle's lifetime. The quantity of data required to be tracked during a particle's lifetime via tallies is not energy-dependent, i.e., the energy of a neutron is constant between any two collision events, so significantly less data need to be stored compared to the IFP method. This makes the CLUTCH method the preferred method for these types of calculations.

Testing of this new capability has been performed by ORNL for several different configurations (i.e., single unit and fuel pins) [4]. The results demonstrate that the IFP method has extremely large computer memory requirements, tending to decrease its usefulness for complex problems such as the HFIR LEU SCALE model. For example, the fuel pin studies using the IFP method demonstrate that it requires significantly more computer memory (2,113 MB) compared to the multigroup TSUNAMI-3D (63 MB) and CLUTCH (0 MB) methods. As previously discussed, the TSUNAMI-3D conventional methodology (multigroup cross sections) did not work even with a significantly simplified model of the HFIR LEU configuration. In contrast, the CLUTCH method performed well and required significantly fewer memory resources than the IFP or conventional methods for the sample problems considered in Reference 4. Therefore, the CLUTCH method was chosen for this work.

The CE TSUNAMI-3D results are compared in this work to direct perturbation (DP) calculations, which involve performing additional analysis in which the number density for a nuclide of interest is changed by a small amount. The k_{eff} results from these analyses are used to manually compute the total sensitivity coefficient, which is compared to the CE TSUNAMI-3D results to ensure that the calculation approach was appropriate for the HFIR LEU core TSUNAMI study.

4. CALCULATIONS AND RESULTS

4.1 HFIR LEU CORE MODEL

A CE TSUNAMI-3D model was created from the KENO-VI HFIR LEU model to generate energy-dependent sensitivity profiles. The SCALE 6.2 Beta 4 package [17] and ENDF/B-VII.1 CE cross section data are used for the TSUNAMI-3D calculations. The model contains number densities for a total of 264 materials [5]. Reference 5 defines the geometric features of the model: the central target region, the fuel and control element regions, the beryllium reflector regions, and the reactor outer regions. Fig. 4 shows a KENO-3D plot of the HFIR LEU core, depicting the inner and outer fuel elements, the beryllium reflector, experiment facilities, and neutron beam tubes. Fig. 5 is a KENO-3D plot of the axial cross section of the HFIR LEU model showing the numerous axial regions in the fuel element region. Fig. 6 is a KENO-3D plot showing the HFIR LEU model inner and outer fuel assemblies, flux trap region, and beryllium reflector.

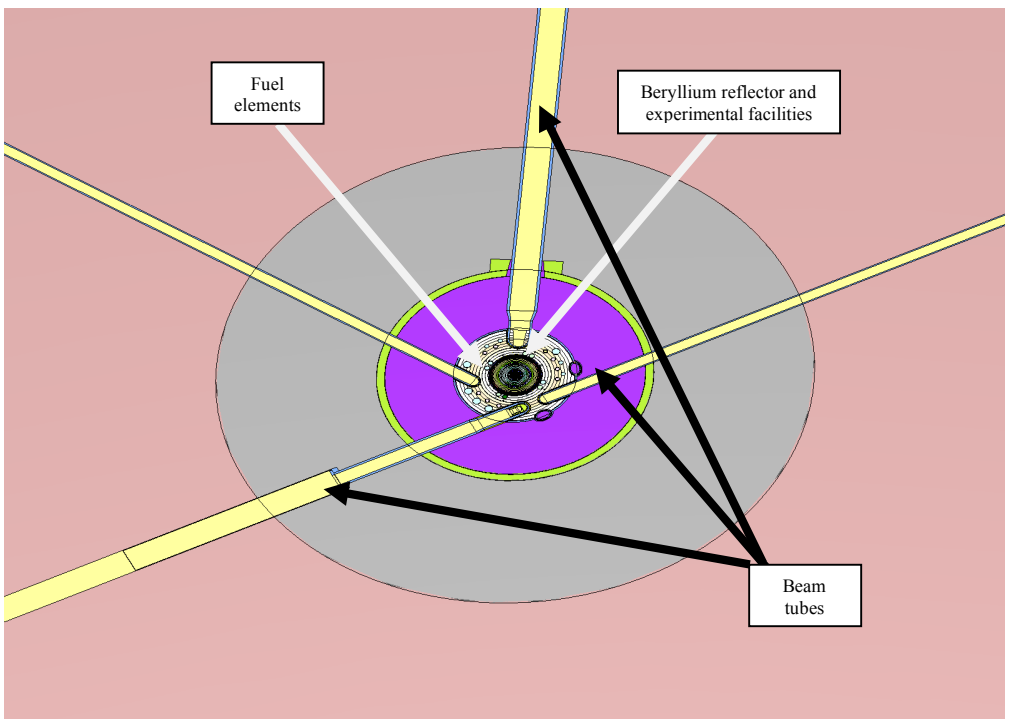

Fig. 4. Cross section of the CE TSUNAMI-3D model for HFIR LEU core.

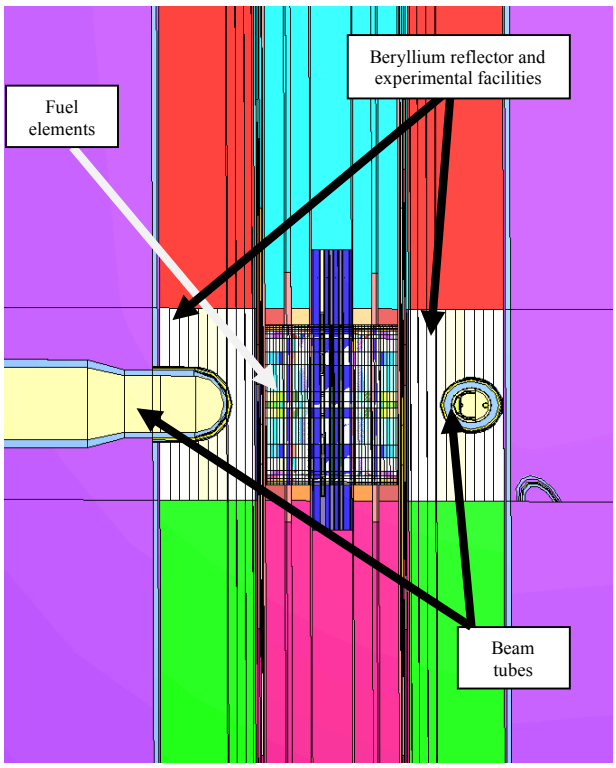

Fig. 5. Axial cross section of the TSUNAMI-3D model for HFIR LEU core.

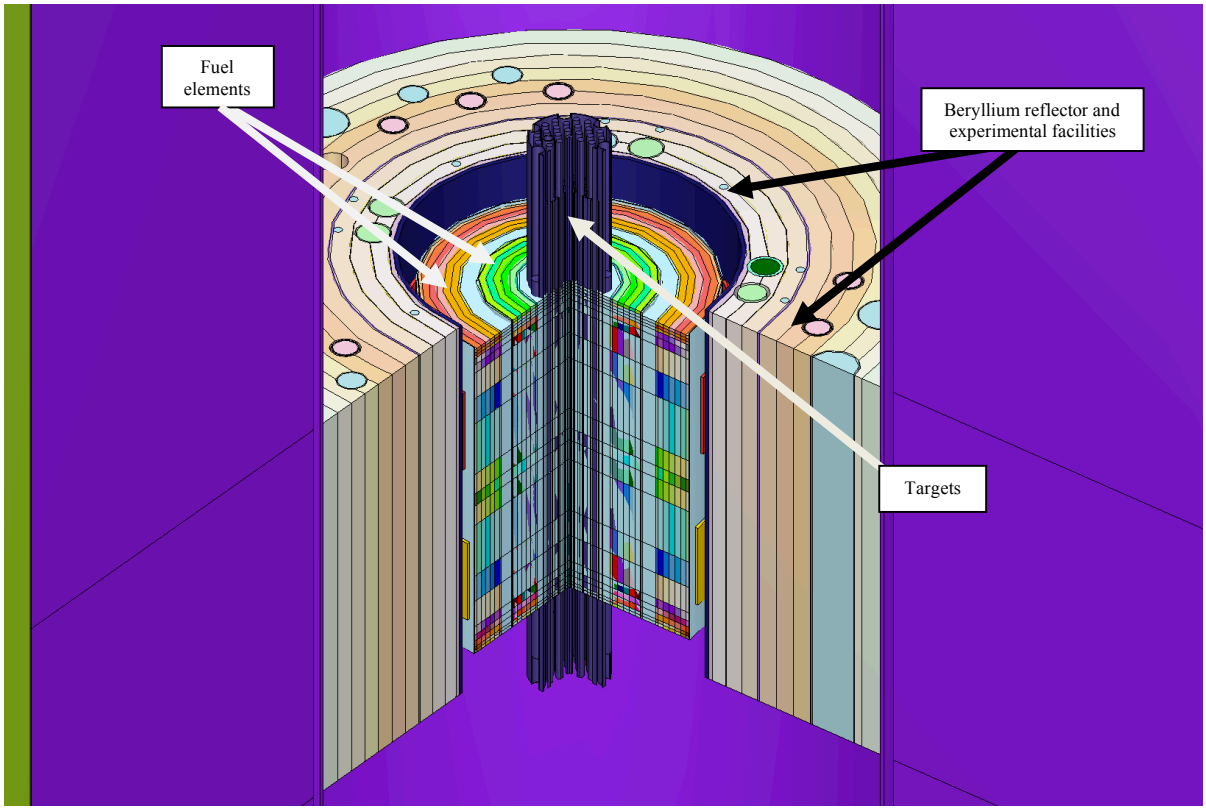

Fig. 6. HFIR LEU core and flux trap region in the LEU Core model.

4.2 TSUNAMI-3D (CE) RESULTS

The goal of this sensitivity analysis is to predict how nuclear data changes affect the k_{eff} of the system. In particular, the sensitivity strategy of TSUNAMI is to estimate the fractional change in k_{eff} caused by a fractional change in the nuclear data. A sensitivity value of 0.1 indicates that a 1% increase in the nuclear cross-section or atom densities will cause a 0.1% increase in the system k_{eff}. For this work, the energy-dependent sensitivity profiles were plotted using a 238-group energy structure. The sensitivity results from the CE TSUNAMI-3D calculations are illustrated in the energy-dependent sensitivity profiles (Fig. 7–Fig. 19) for ^{1}H, ^{9}Be bound, ^{235}U, ^{238}U, and molybdenum (^{92}Mo, ^{94}Mo, ^{95}Mo, ^{96}Mo, ^{97}Mo, ^{98}Mo, and ^{100}Mo). These nuclides produced the largest k_{eff} sensitivities. The sensitivity results produced by CE TSUNAMI-3D are defined as $(\delta k/k)/(\delta\Sigma/\Sigma)$ and are unitless values.

Table 1 shows a summary of the energy-integrated TSUNAMI-3D CE results for the aforementioned nuclides as a function of reaction type. Table 1 shows how the CE TSUNAMI results compare to direct perturbation calculations (discussed in more detail in 4.3). Energy dependent sensitivity results are shown in the sensitivity profiles in Fig. 7-Fig. 19.

Table 1. Energy-integrated sensitivities and standard deviations for HFIR loaded with LEU fuel

Isotope	Reaction	Direct perturbation		CE TSUNAMI-3D	
		S[a]	σ_S[b]	S[a]	σ_S[b]
^{9}Be (Be bound)	Total	4.550E-02	2.994E-04	4.743E-02	9.521E-04
	Elastic scatter			4.240E-02	9.507E-04
	Capture			-4.401E-03	1.421E-06
	n,2n			9.429E-03	9.382E-06
^{1}H	Total	2.212E-01	1.406E-03	2.223E-01	1.503E-03
	Elastic Scatter			2.685E-01	1.504E-03
	Capture			-4.617E-02	6.292E-06
^{235}U	Total	1.431E-01	9.238E-04	1.442E-01	4.693E-05
	Elastic Scatter			1.275E-03	3.263E-05
	Capture			-1.635E-01	1.683E-05
	Fission			3.044E-01	3.537E-05
	n,n'			1.965E-03	1.154E-05
^{238}U	Total	-3.660E-02	2.393E-04	-3.692E-02	1.086E-04
	Elastic Scatter			1.299E-02	9.719E-05
	Capture			-7.969E-02	1.114E-05
	Fission			1.902E-02	1.410E-05
	n,n'			1.024E-02	2.915E-05
Mo	Capture	-1.190E-02	7.573E-05	-1.180E-02	4.141E-05
^{95}Mo[c]	Capture	NC[d]	NC	-1.055E-02	2.739E-06

[a] S = energy integrated sensitivity results
[b] σ_S = standard deviation of the energy integrated sensitivity results
[c] The integral sensitivities for ^{92}Mo, ^{94}Mo, ^{96}Mo, ^{97}Mo, ^{98}Mo, and ^{100}Mo capture are small compared to ^{95}Mo capture sensitivity results and are not provided here but are provided in the energy-dependent sensitivity profiles in Fig. 18. The results for Mo nuclide inelastic scattering sensitivity results are also very small (~10^{-4}) and are not provided here but are provided in Fig. 17.
[d] Not calculated

The energy-dependent sensitivity profiles for ^{1}H for the total, capture, and elastic scattering cross-section are shown in Fig. 7. The total cross section sensitivity for ^{1}H includes contributions from both capture and scattering reactions. The sensitivity results for ^{1}H indicate that the k_{eff} is sensitive to ^{1}H capture and, to a lesser extent, elastic scattering at ~0.06 eV. There are some positive sensitivity peaks for ^{1}H elastic scattering for 1-110 eV and at approximately 1-2 MeV; however, there are no sensitivities noted for ^{1}H capture over these ranges. The maximum sensitivity for ^{1}H total (sum of sensitivity contributions for ^{1}H

elastic scattering and ^{1}H capture) occurs at about 7 eV (~0.14) with smaller sensitivity peaks between 7-110 eV. There is a negative sensitivity peak ^{1}H total at about 0.05 eV (-0.044).

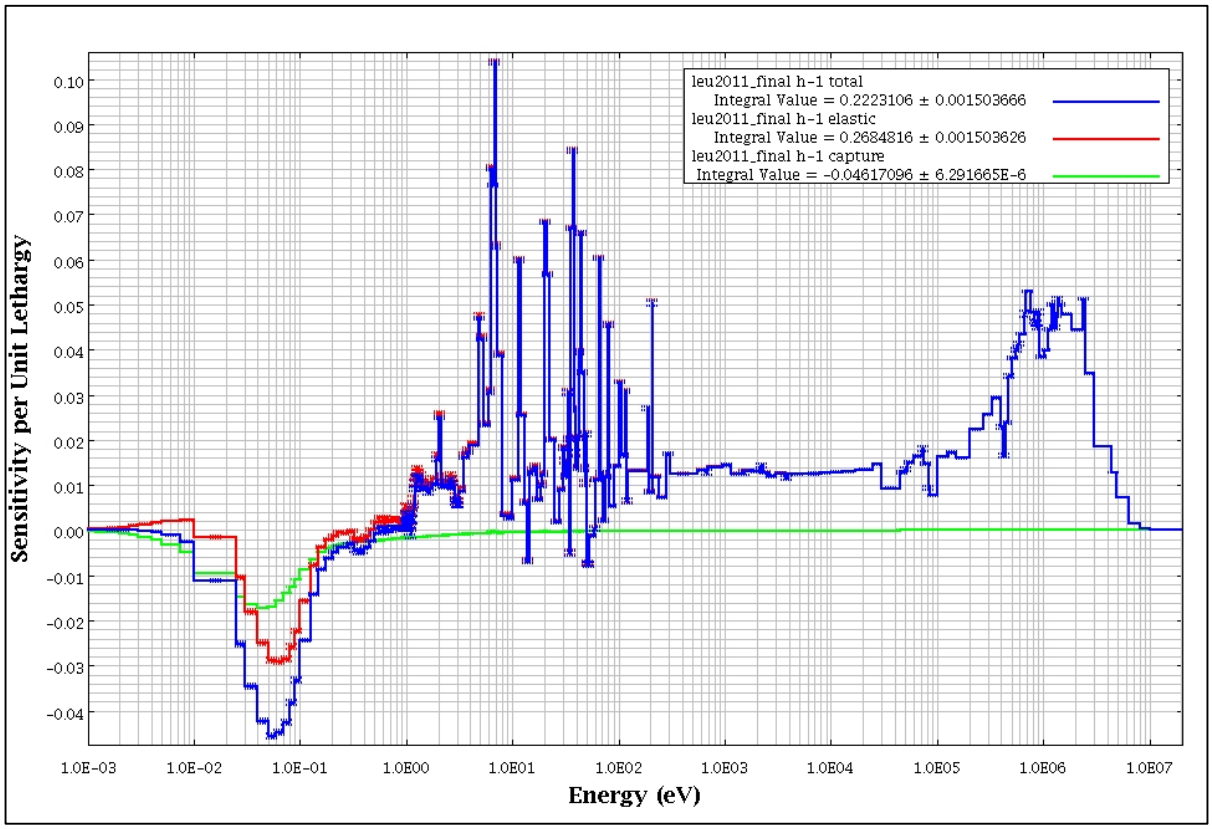

Fig. 7. Energy-dependent sensitivity profiles for ^{1}H (capture, elastic scatter, and total).

The energy-dependent sensitivity profiles for ^{9}Be are shown in Fig. 8. The profiles show two small negative sensitivities for ^{9}Be capture at about 0.04 eV and about 2 MeV. The profiles indicate a small negative sensitivity at about 0.08 eV for ^{9}Be elastic scattering. There are some positive sensitivities peaks between about 3 eV – 1 keV and a significant sensitivity peak at about 2 MeV for ^{9}Be elastic scattering. The sensitivities to ^{9}Be capture are small. Fig. 9 shows the energy-dependent sensitivity profile for ^{9}Be (n,2n) reactions. For neutron energies below about 2 MeV, the cross section for ^{9}Be(n,2n) is essentially zero. Above 2 MeV, the cross section increases significantly to about 0.32 barns (Fig. 10) and is relatively constant above about 5 MeV (based on ENDF/B-VII cross section data). Fig. 9 indicates that there is a small sensitivity peak at about 3 MeV, approximately where the ^{9}Be (n,2n) threshold is for the ^{9}Be (n,2n) cross section.

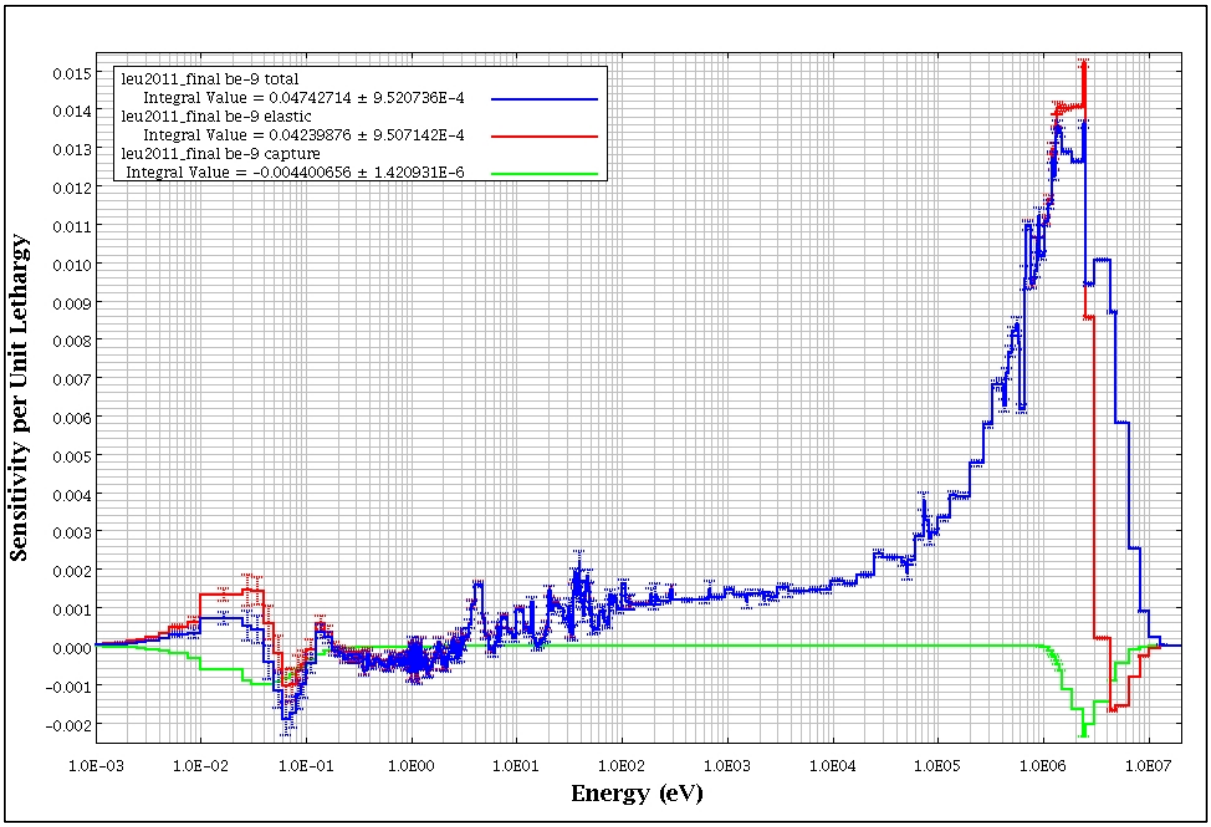

Fig. 8. Energy-dependent sensitivity profiles for ^{9}Be (capture, elastic scatter, and total).

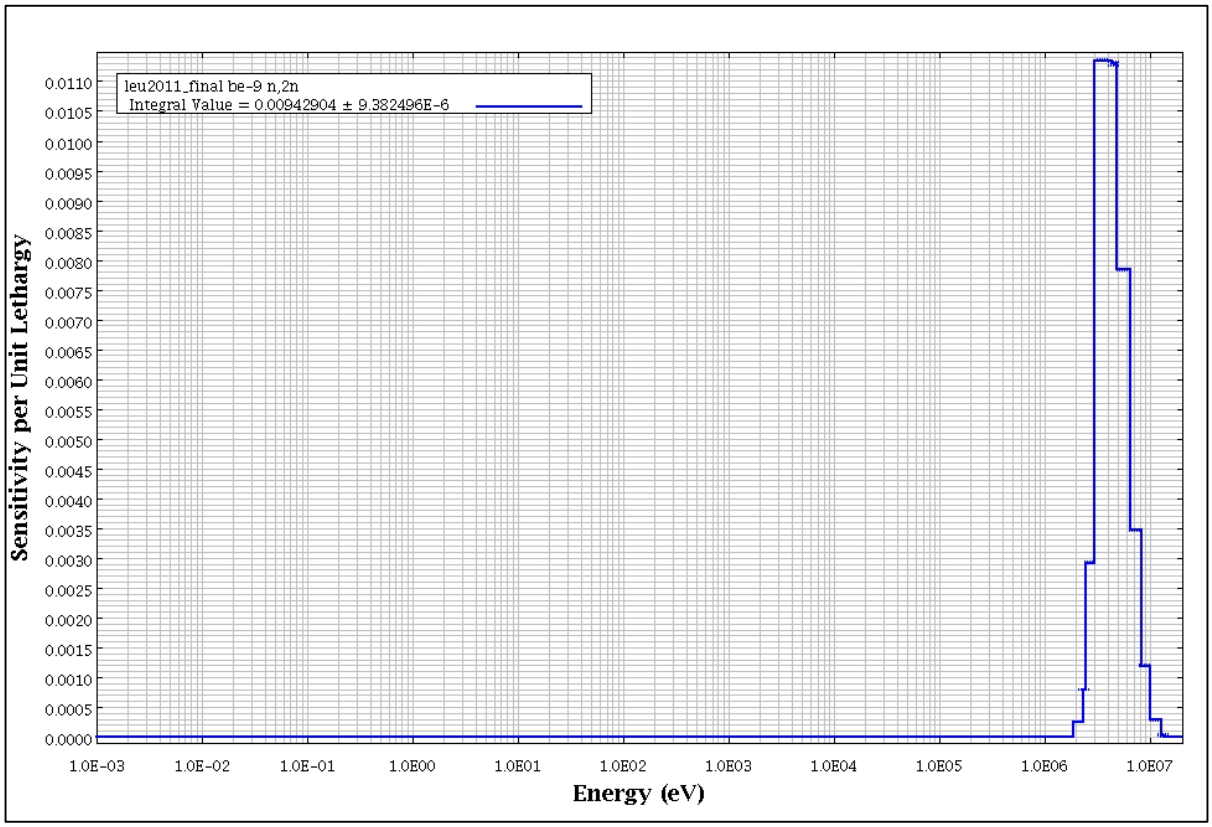

Fig. 9. Energy-dependent sensitivity profile for 9Be(n,2n).

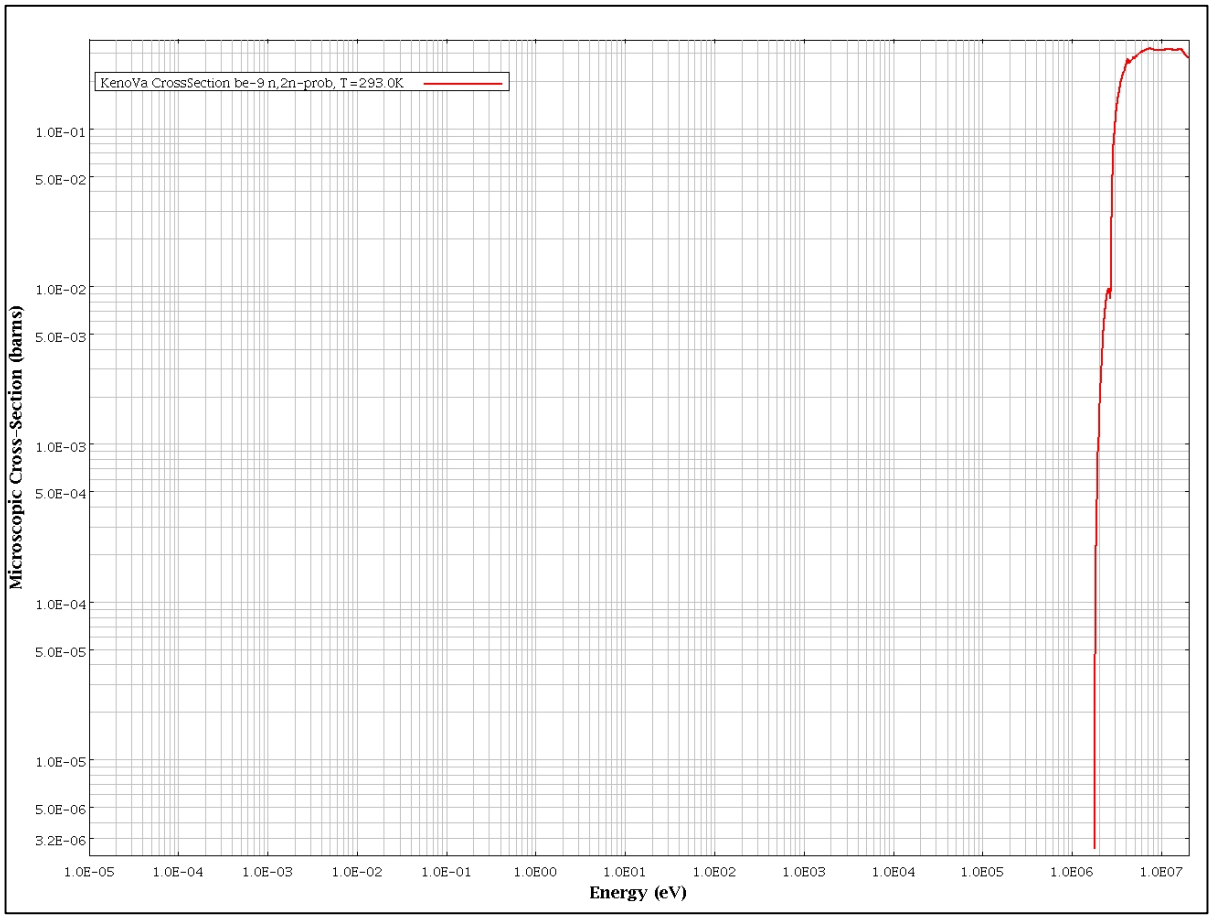

Fig. 10. Neutron cross section for ^{9}Be(n,2n) reaction.

Fig. 11 shows the energy-dependent sensitivity profiles for ^{235}U fission, capture, elastic scattering, and total. For ^{235}U elastic scattering, the sensitivity of the k_{eff} to small changes in the elastic scattering cross section as a function of energy is essentially zero. For ^{235}U fission, there is a region of positive sensitivity at about 0.05 eV, numerous positive peaks from ~1 eV to about 1 keV (maximum peak at ~0.3 eV), and a small region of positive sensitivity at about 2 MeV. For ^{235}U capture, there is a region of small, negative sensitivity at about 0.06 eV and numerous negative sensitivity peaks from about 1 eV to about 1 keV.

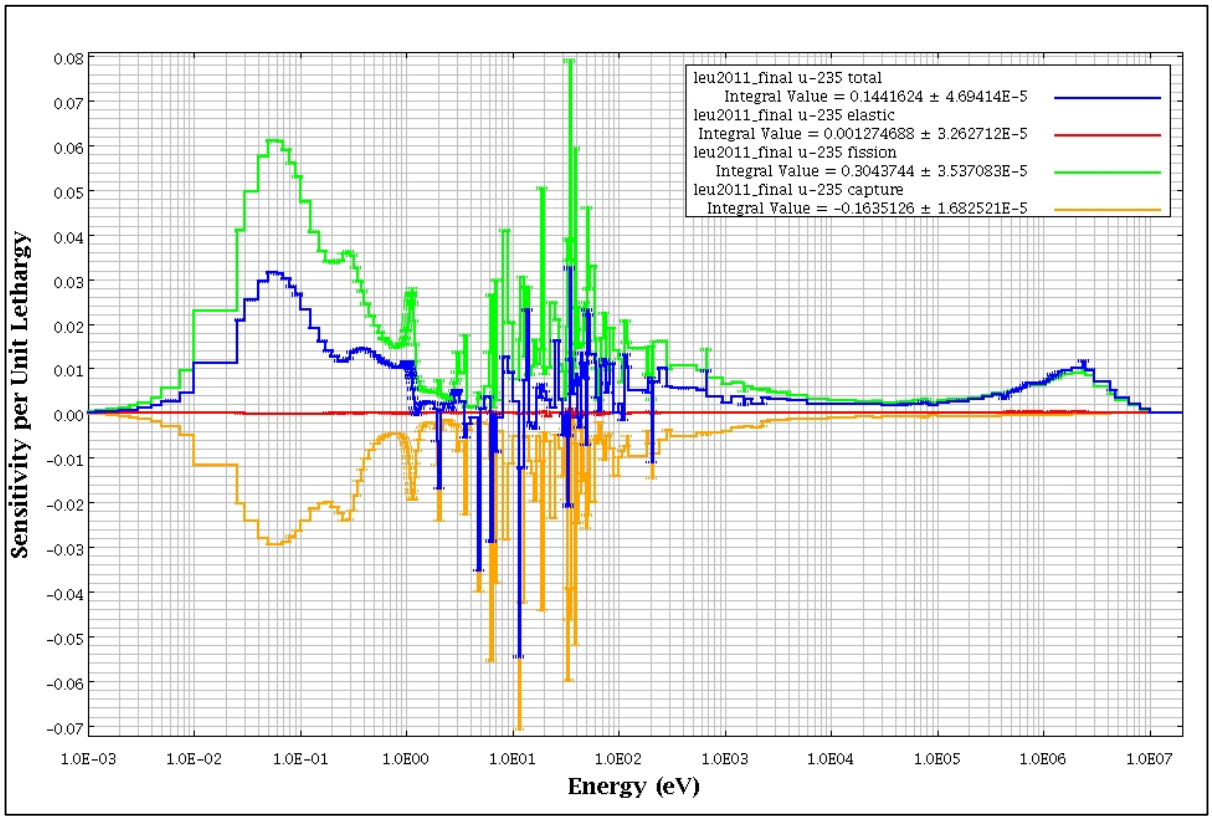

Fig. 11. Energy-dependent sensitivity profiles for ^{235}U (capture, elastic scatter, total, and fission).

Fig. 12 illustrates the energy-dependent sensitivity profile for the ^{235}U (n, n') reaction (inelastic scattering). Because inelastic scattering is a threshold reaction, the sensitivity of the system k_{eff} to ^{235}U (n, n') is near zero until about ~2 MeV, where this reaction sensitivity peaks. The sensitivity of k_{eff} to ^{235}U inelastic scattering is much smaller than the sensitivities to ^{235}U capture, scatter, and fission reactions.

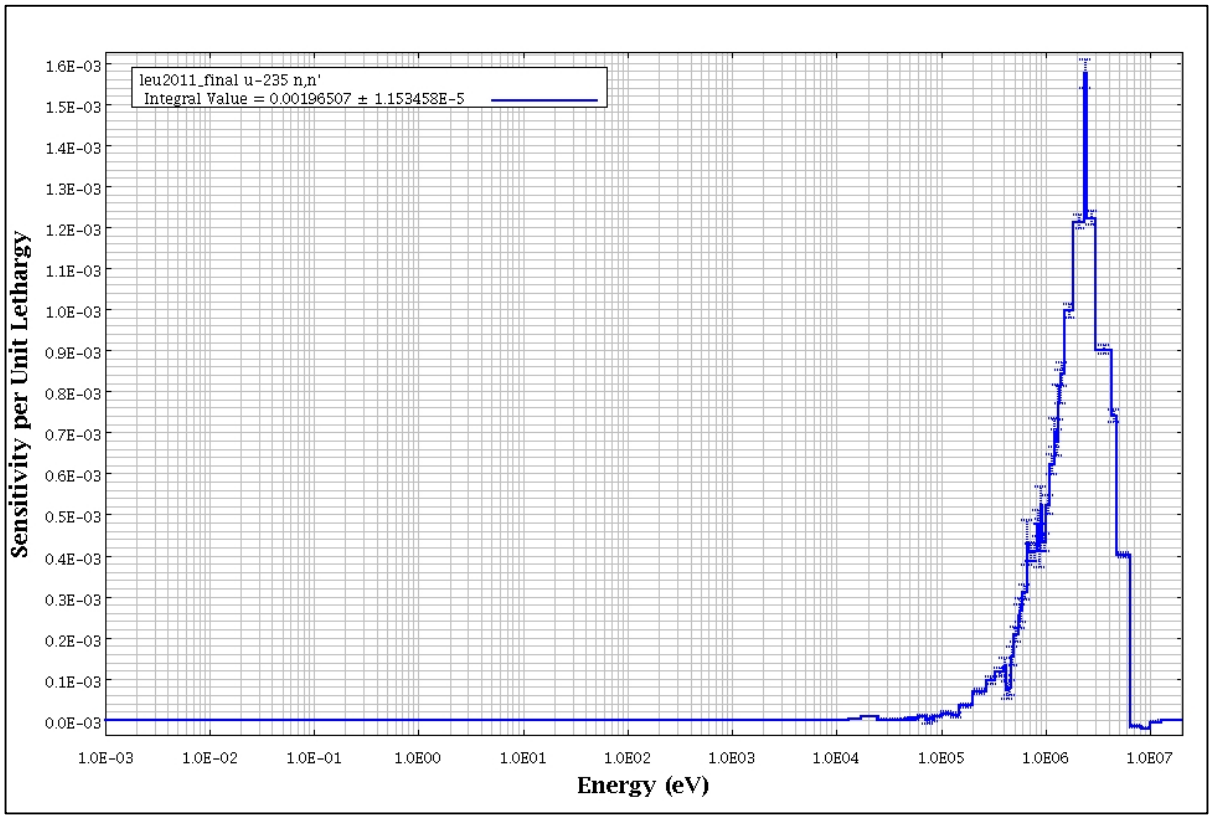

Fig. 12. Energy-dependent sensitivity profile for ^{235}U inelastic scattering (n,n').

Fig. 13 shows the energy-dependent sensitivity profiles for ^{238}U capture, elastic scatter, fission, and total. The profiles for each reaction in the thermal region of the fission and elastic scattering reactions are essentially zero up to about 0.06 eV where the net sensitivities are negative (primarily from ^{238}U fission) but very small (about -0.004 or less). From 6 eV to 10 keV, there are numerous negative sensitivity peaks for ^{238}U capture and numerous positive sensitivity peaks for ^{238}U elastic scattering (smaller in magnitude than the capture sensitivities). This makes sense, because of the number and magnitude of the capture resonances for ^{238}U could be the source of cross section uncertainties in this neutron energy range (intermediate energy/resonance energy range). There is also a relatively small positive sensitivity peak at about 2 MeV for ^{238}U fission. Above ~10 keV, there are no significant sensitivity peaks for ^{238}U scattering and capture (nonfission).

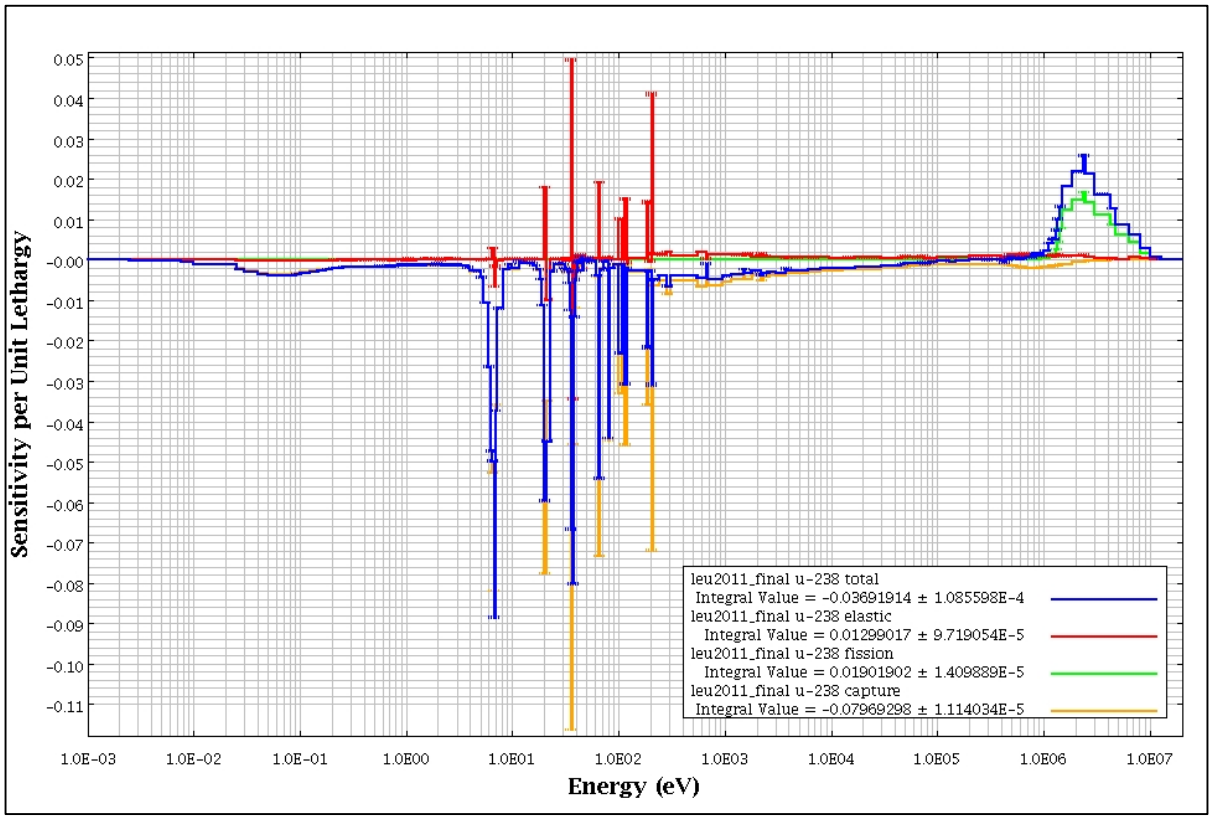

Fig. 13. Energy-dependent sensitivity profiles for ^{238}U (capture, elastic scatter, total, and fission).

Fig. 14 shows the energy-dependent sensitivity profile for ^{238}U inelastic scattering (n,n'). Inelastic scattering is a threshold reaction, so the sensitivity results below about 1 MeV are near zero as expected. There is a positive sensitivity to ^{238}U (n, n') on the system k_{eff} at about 2.0 MeV, which is relatively small compared to other ^{238}U reaction sensitivities discussed previously.

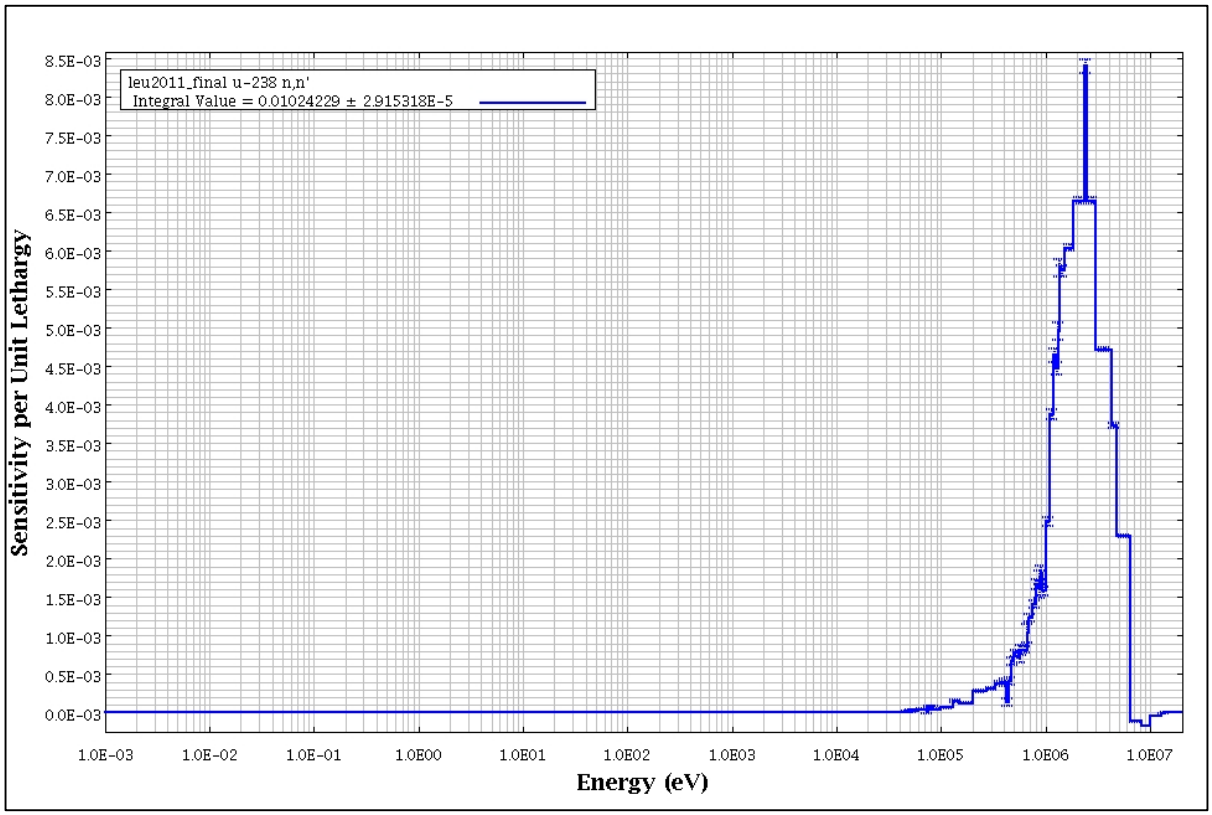

Fig. 14. Energy-dependent sensitivity profile for ^{238}U inelastic scattering (n,n').

Fig. 15 shows the energy-dependent sensitivity profiles for ^{92}Mo, ^{94}Mo, ^{96}Mo, ^{97}Mo, ^{98}Mo, and ^{100}Mo for elastic scattering. Molybdenum is a significant constituent (~10% by weight) of the HFIR LEU fuel meat that is present in the plates of the inner and outer fuel elements. The magnitude of the total molybdenum sensitivity is dominated by the elastic reaction for ^{96}Mo, although the sensitivity of system k_{eff} to small perturbations in the molybdenum density is relatively small. There is a sharp positive sensitivity peak for ^{96}Mo elastic scattering at about 200 eV, but the magnitude of the sensitivity is rather small. There are some very small k_{eff} sensitivities throughout the sensitivity profiles, as indicated in the intermediate neutron energy range and at about 1 MeV. Overall, the molybdenum elastic scattering sensitivity results for these isotopes are very small, less than 10^{-3}, and are essentially negligible.

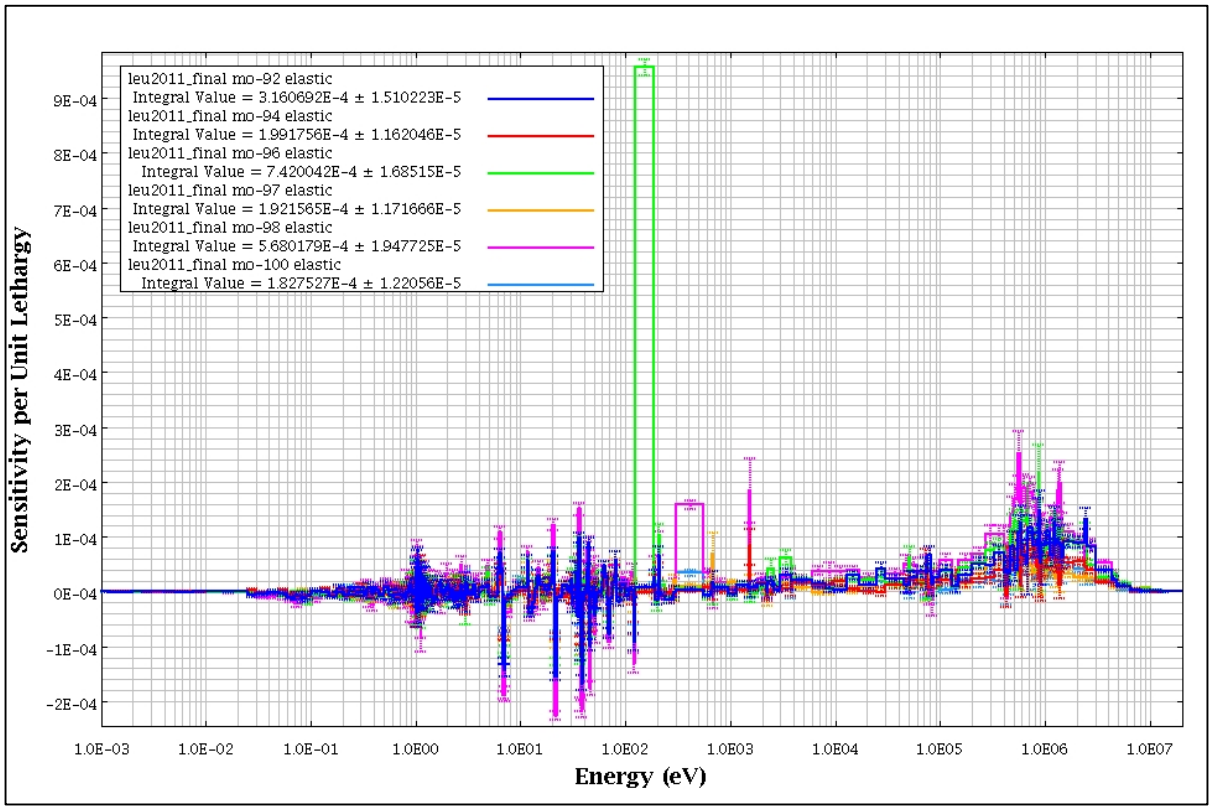

Fig. 15. Energy-dependent sensitivity profiles for various molybdenum isotopes (elastic scatter).

The energy-dependent sensitivity profiles for ^{95}Mo elastic scattering are shown in Fig. 16. There is a significant positive sensitivity peak of magnitude ~ 0.04 at about 4 eV followed by a small negative peak at just above 4 eV. The sensitivity of the k_{eff} to small changes in the ^{95}Mo elastic scattering cross section as a function of energy is essentially zero both below and above 4 eV.

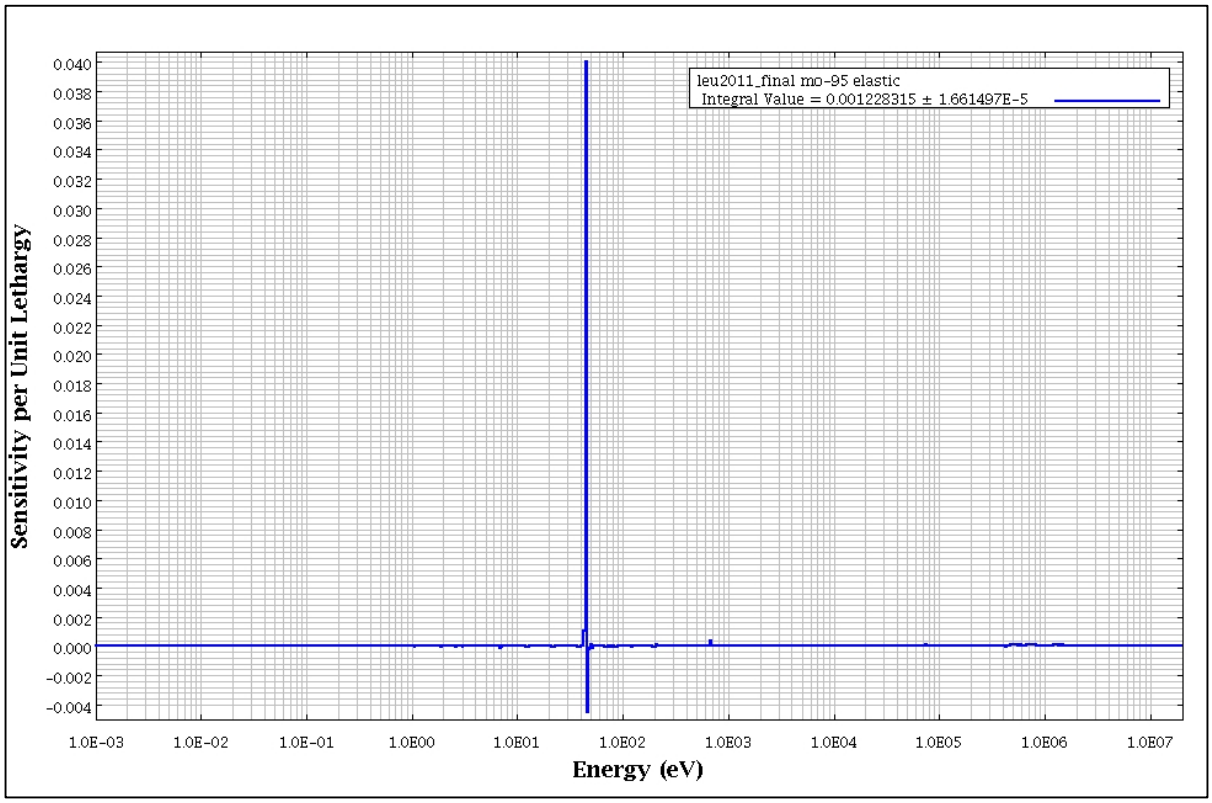

Fig. 16. Energy-dependent sensitivity profiles for ^{95}Mo (elastic scattering).

Fig. 17 shows the energy-dependent sensitivity profiles for ^{92}Mo, ^{94}Mo, ^{95}Mo, ^{96}Mo, ^{97}Mo, ^{98}Mo, and ^{100}Mo inelastic scattering (n,n'). As mentioned previously for ^{238}U, inelastic scattering is a threshold reaction, so it is not unreasonable for the sensitivity results below about 1 MeV to be zero. There is a positive sensitivity to k_{eff} to all the molybdenum isotopes for inelastic scattering at about 2.0 MeV with ^{98}Mo and ^{95}Mo dominating the positive sensitivity peak. The integral sensitivities for ^{98}Mo and ^{95}Mo inelastic scattering dominate the other molybdenum isotopes. The k_{eff} sensitivities for the molybdenum isotopes for perturbations in the inelastic scattering nuclear data are very small, less than 4×10^{-4}.

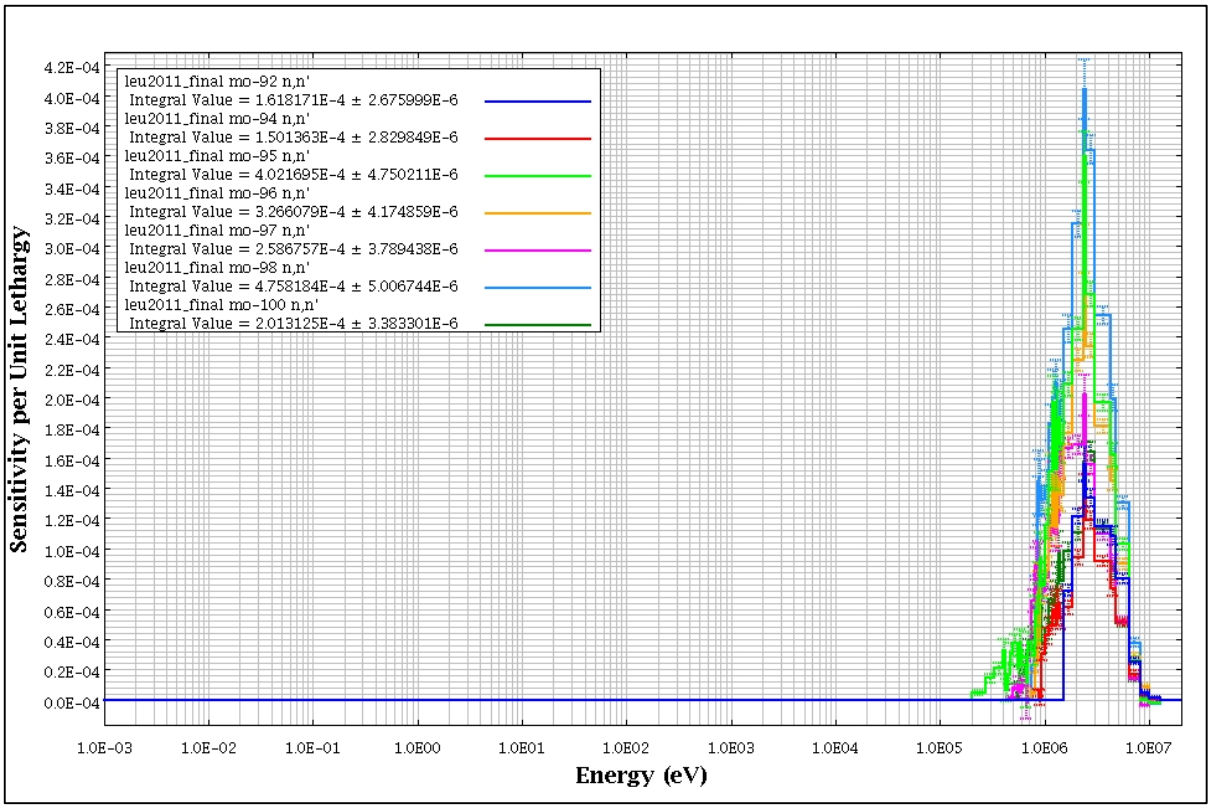

Fig. 17. Energy-dependent sensitivity profiles for various molybdenum isotopes (inelastic scattering).

Fig. 18 shows the energy-dependent sensitivity profiles for ^{92}Mo, ^{94}Mo, ^{96}Mo, ^{97}Mo, ^{98}Mo, and ^{100}Mo capture. There are negative k_{eff} sensitivities for perturbations in the capture cross sections for all molybdenum isotopes. The magnitude of the sensitivity results shown in Fig. 18 are an order of magnitude larger than the elastic and inelastic scatting sensitivity results. Even so, the k_{eff} sensitivity results for molybdenum capture are very small, less than 8×10^{-3} in absolute value.

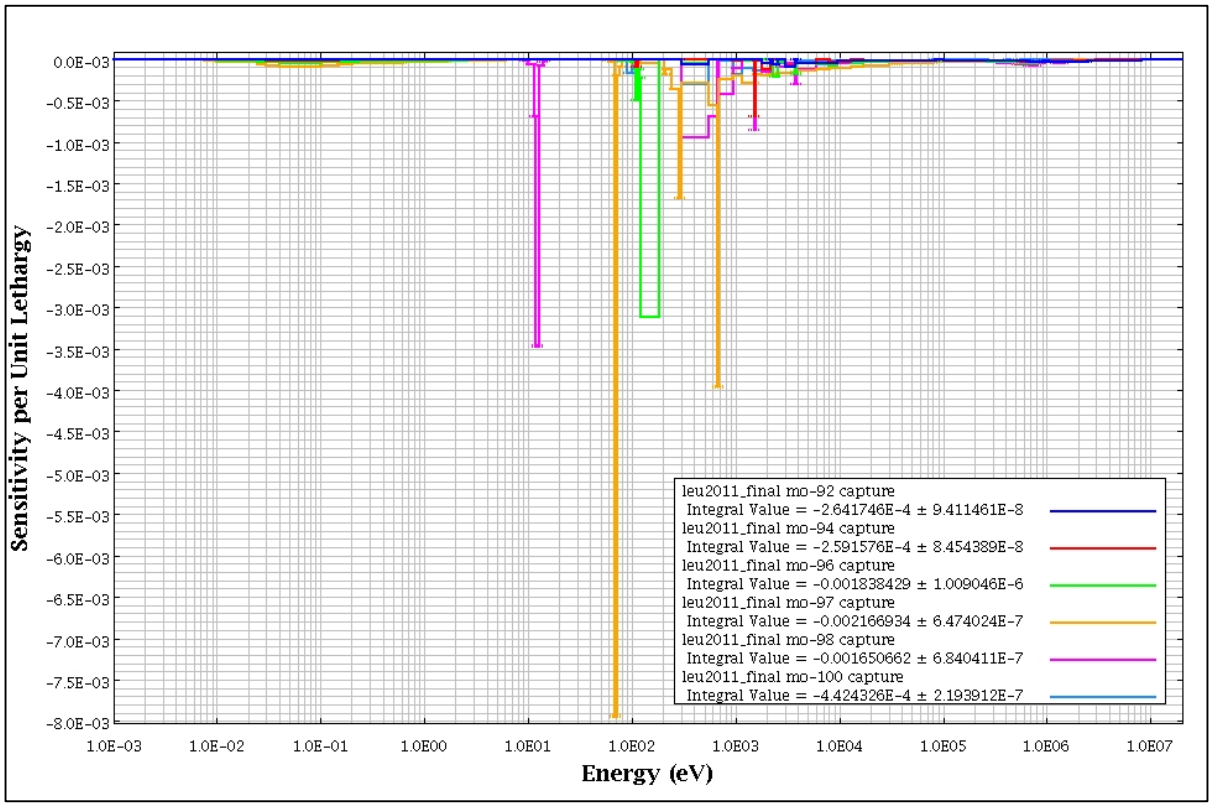

Fig. 18 Energy-dependent sensitivity profiles for various molybdenum isotopes (capture).

Fig. 19 shows the energy-dependent sensitivity profiles for ^{95}Mo capture. The k_{eff} has a negative sensitivity to the ^{95}Mo cross section of ~0.11 at about 40 eV that is significantly larger in magnitude than all the other molybdenum isotopes considered in Fig. 18. The sensitivity profile for ^{95}Mo capture is essentially zero elsewhere.

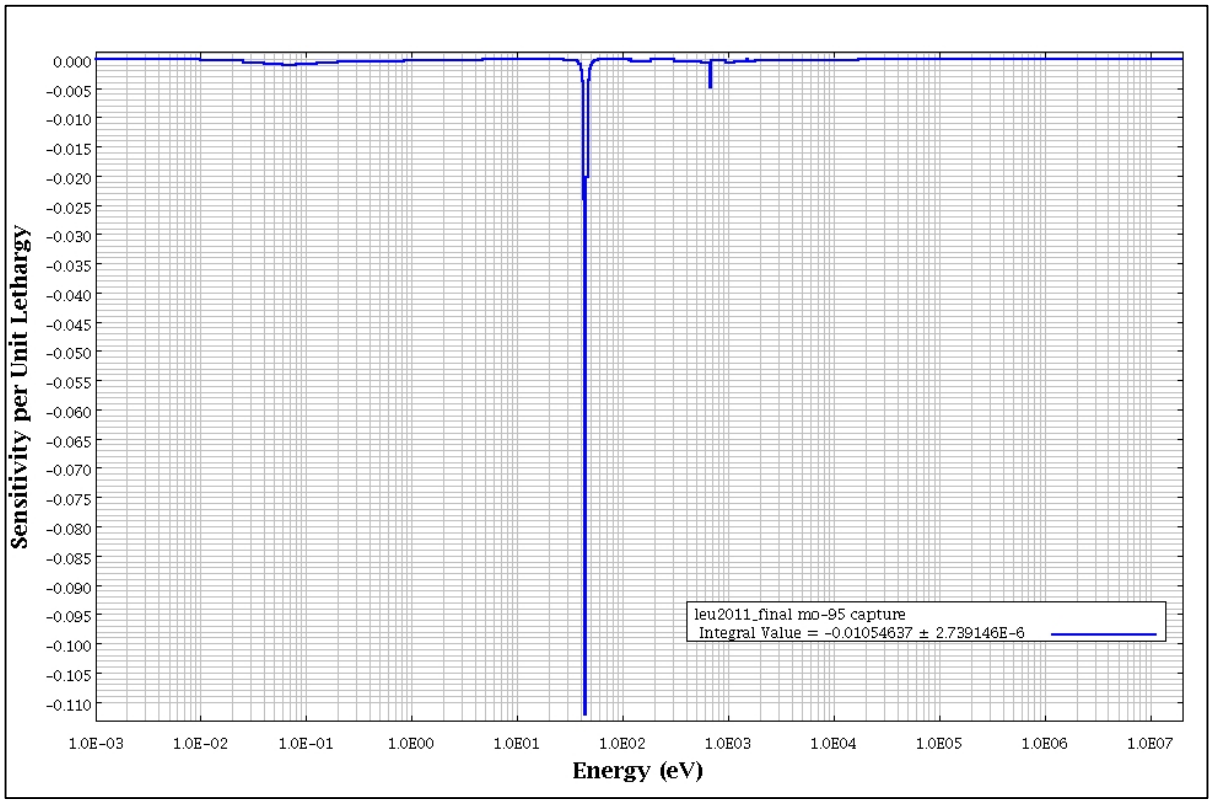

Fig. 19. Energy-dependent sensitivity profiles for ^{95}Mo (capture).

4.3 DIRECT PERTURBATION CALCULATIONS

It is important to check the sensitivity coefficients generated by TSUNAMI-3D for the HFIR LEU core model. It has been noted in the past that the TSUNAMI-3D results can vary significantly, depending upon the calculation input parameters and modeling assumptions with respect to the cross section processing (resonance self-shielding calculations) and criticality calculations. The sensitivity results performed here are verified by comparing them with DP calculations. DP calculations involve perturbation of the HFIR model input parameters, in this case material densities. DP calculations [18, 19] for this work involve computing the system k_{eff} with nominal values of the material density then with a selected input value increased by a certain percentage and then with the value decreased by the same percentage.

The DP results in this work are shown in Table 2 for the isotopes of interest and compares the calculated sensitivity (S) and standard deviation of the sensitivity (σ_S) for CE TSUNAMI and the DP HFIR cases. The sensitivity results in Table 1 are the energy-integrated sensitivities instead of the energy-dependent sensitivities previously discussed. The DP calculations results are illustrated in Fig. 20−Fig. 24 for a percentage change in the material density (assumed to be +/- 1% for these calculations). The figures show the relationship between the ratio of the original material density, ρ_0, and the perturbed material density, ρ, and the ratio of the final k_{eff}, k, and the original k_{eff}, k_0. The data in these figures indicate linear behavior between these parameters for the isotopes of interest, which indicates acceptable DP results. These calculations helped to identify some technical issues with the code package and SCALE execution sequences that were resolved as this work proceeded. The results, shown in Table 2, indicate good agreement for the ^{9}Be, ^{1}H, Mo, ^{235}U and ^{238}U total sensitivities between the TSUNAMI and DP calculations, with corresponding relative differences of 4.12%, 0.49%, -1.39%, 0.75%, and 0.91%,

respectively. The relative differences are less than two standard deviations, and the absolute differences are smaller than 0.002.

For multigroup TSUNAMI-3D, one indicator for determining if the TSUNAMI-3D data are acceptable is to ensure that the difference between the forward and adjoint k_{eff} results for the simplified model was less than about 0.5% Δk. For CE TSUNAMI-3D, the adjoint calculation is not performed, so only a comparison of the CE TSUNAMI results to the DP results can provide the analyst with some assurance that the code package is performing as intended. Because of significant memory limitations on the computer systems running the multigroup version of TSUNAMI-3D, the HFIR LEU KENO-VI model would not successfully execute. Obviously, the CE TSUNAMI-3D package allowed this analysis to be completed with no significant computer memory issues. The DP calculations compare well to the CE TSUNAMI results.

Table 2. Comparison of CE TSUNAMI and direct perturbation results

Isotope	CE TSUNAMI			Direct Perturbation			Comparison		
	S[a]	σ_S[b]	$\%\sigma_S$	S	σ_S	$\%\sigma_S$	% difference[c]	standard deviation difference[d]	difference[e]
Be bound (^{9}Be)	0.0474	9.521E-04	2.01	0.0455	2.994E-04	0.66	4.18	1.90	0.00190
^{1}H	0.2223	1.504E-03	0.68	0.2212	1.406E-03	0.64	0.50	0.53	0.00110
Mo	-0.0118	4.141E-05	0.35	-0.0119	7.573E-05	0.64	-0.84	1.16	0.00010
^{235}U	0.1442	4.694E-05	0.03	0.1431	9.238E-04	0.65	0.77	1.19	0.00110
^{238}U	-0.0369	1.086E-04	0.29	-0.0366	2.393E-04	0.65	0.82	1.14	-0.00030

[a] S = energy integrated sensitivity results

[b] σ_S = standard deviation of the energy integrated sensitivity results

[c] % difference = $\frac{(S_{TSUNAMI\text{-}3D}-S_{DP})}{S_{DP}}*100\%$

[d] standard deviation difference = $\left|\frac{(S_{TSUNAMI\text{-}3D}-S_{DP})}{\sqrt{\sigma_{TSUNAMI\text{-}3D}^2+\sigma_{DP}^2}}\right|$

[e] difference = $S_{TSUNAMI\text{-}3D} - S_{DP}$

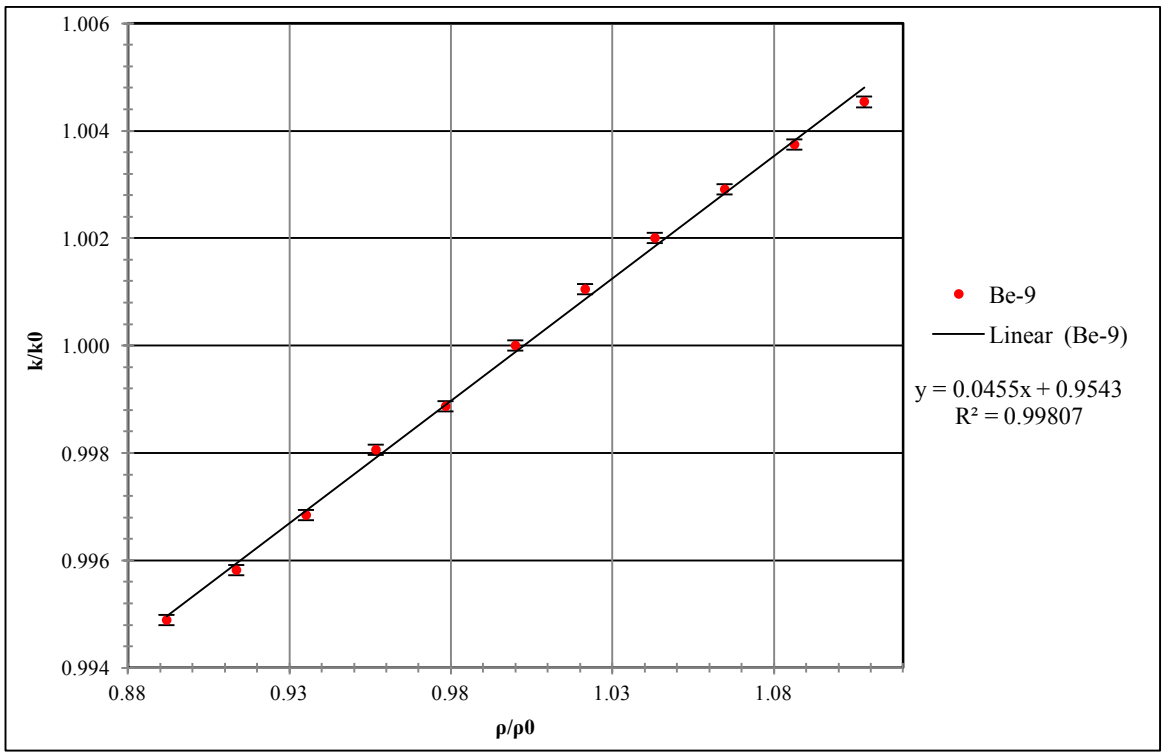

Fig. 20. Graphical DP results for ^{9}Be bound.

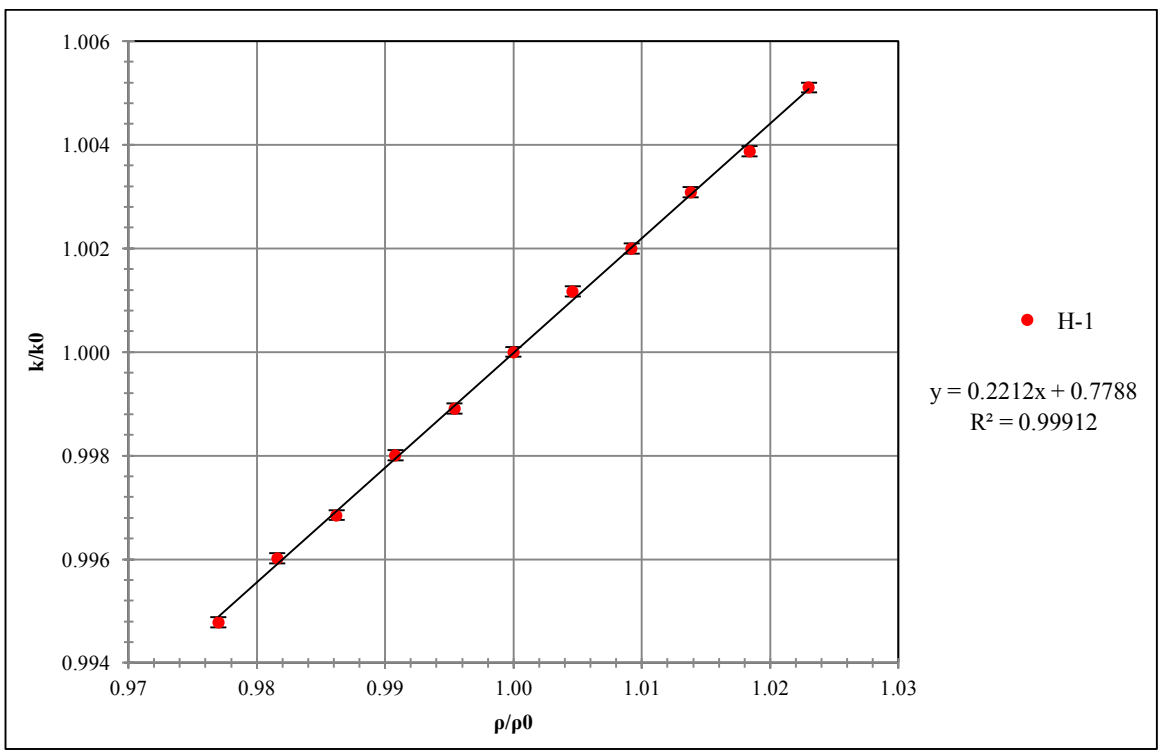

Fig. 21. Graphical DP results for ^{1}H.

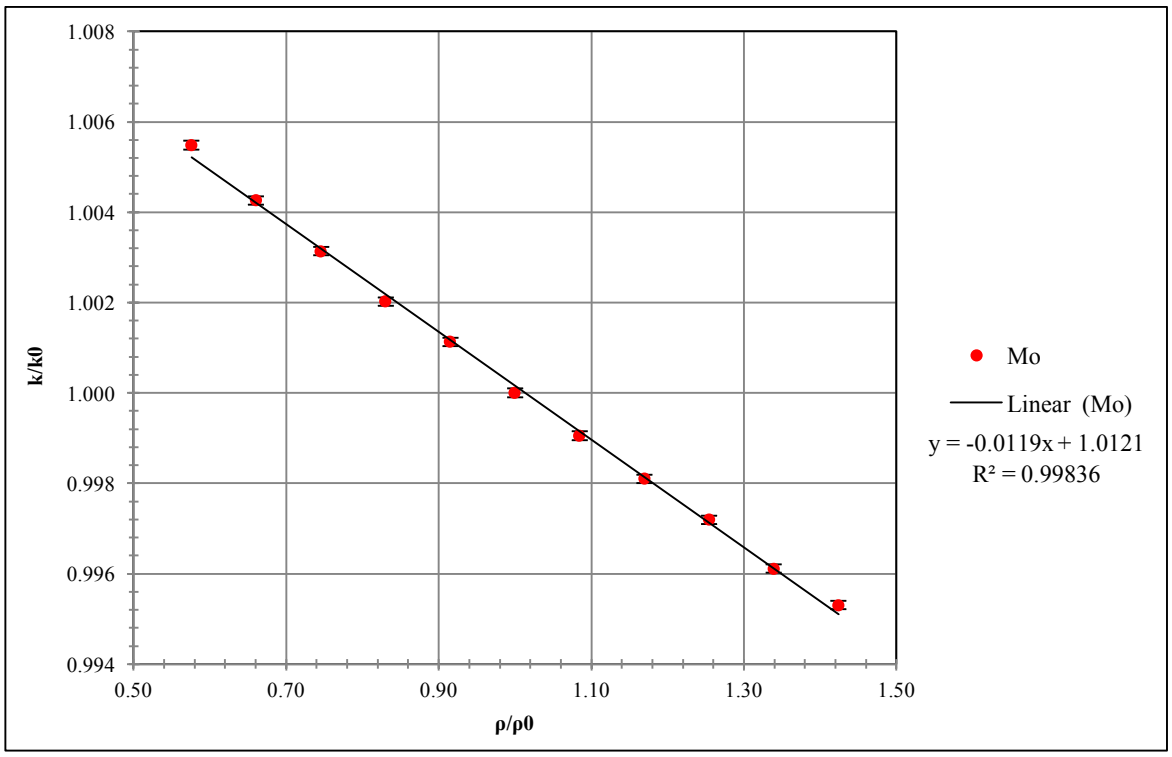

Fig. 22. Graphical DP results for Mo.

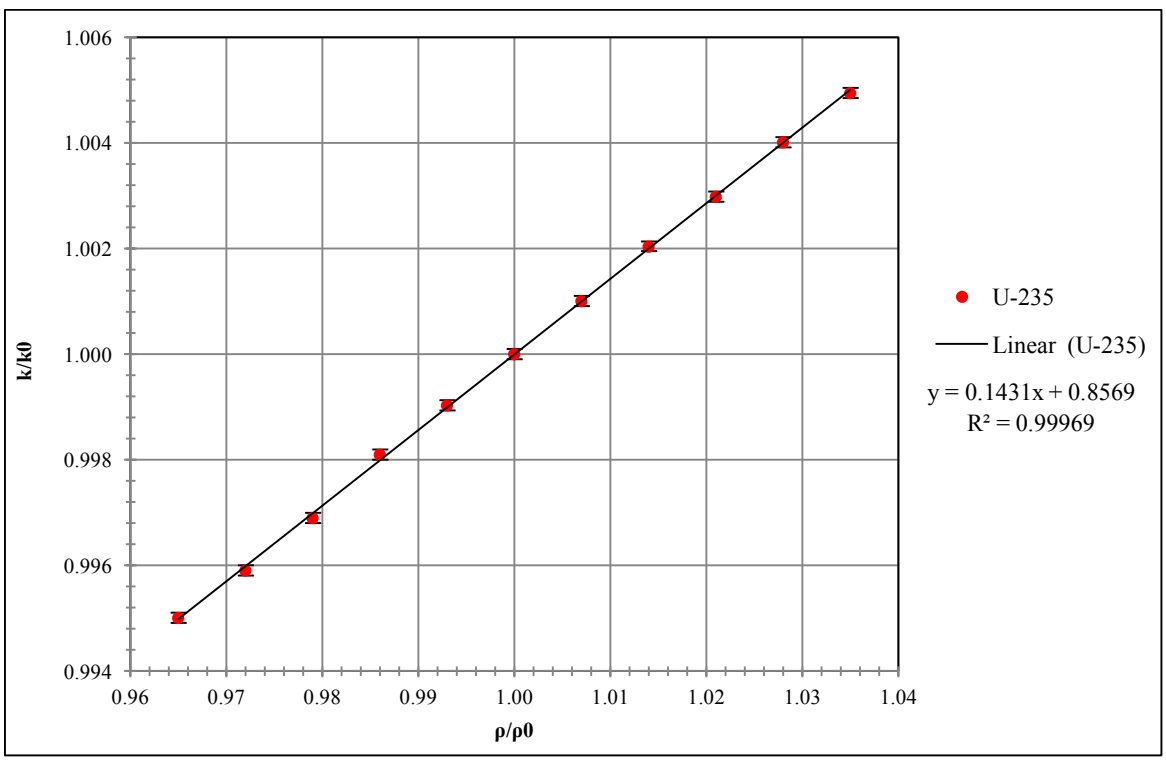

Fig. 23. Graphical DP results for ^{235}U.

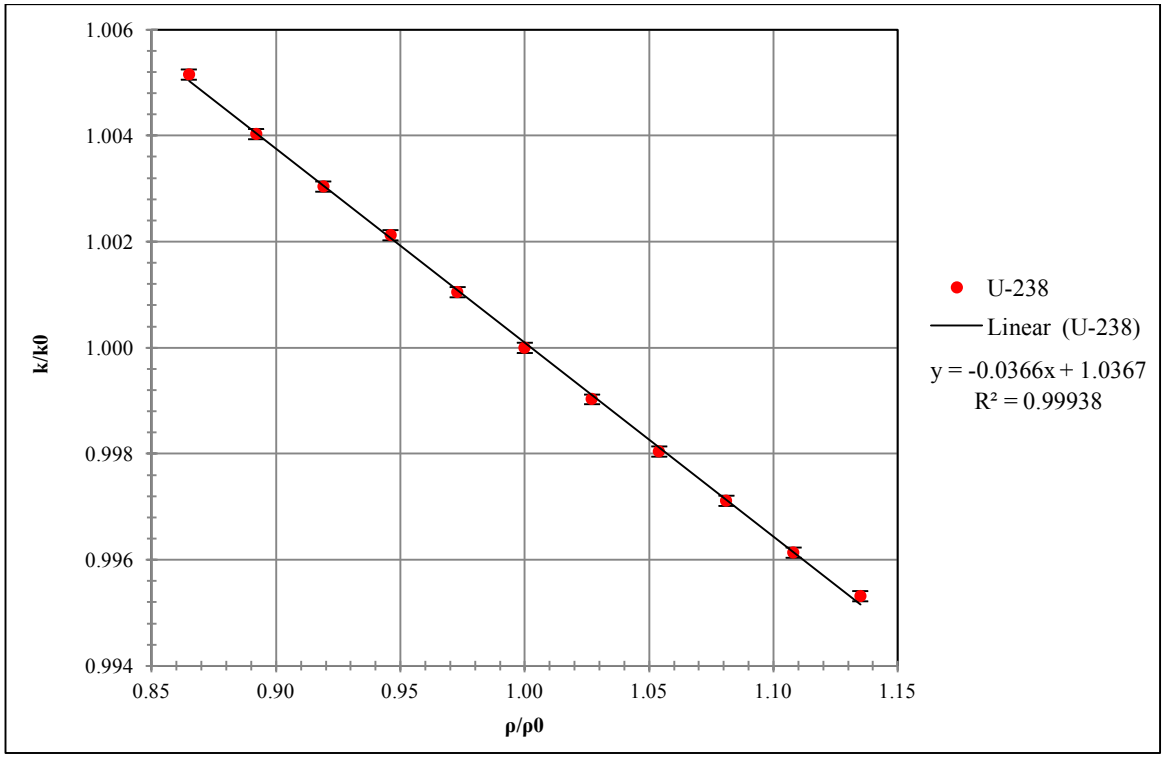

Fig. 24. DP Graphical results for ^{238}U.

4.4 CE TSUNAMI CALCULATION DISCUSSION

The results of the sensitivity analysis show that the two largest integral sensitivities are with ^{1}H elastic scattering at 0.269 and ^{235}U fission at 0.304 (Table 1). There is a significant negative sensitivity (0.01 – 1.0 eV) and positive sensitivity peaks from Fig. 7 in the resonance and fast neutron energy regions to small variations in the ^{1}H cross sections due to elastic scattering reactions resulting from neutron moderation.

Fig. 11 shows a significant positive sensitivity to the system k_{eff} to ^{235}U fission at thermal (~0.1 eV) and over the resonance range, indicating that the HFIR LEU core has a positive sensitivity to perturbations in the ^{235}U fission cross section in the core of the reactor, which is not unexpected. There are also significant negative sensitivity peaks for ^{235}U capture at thermal and over the resonance range, although the magnitude of these sensitivities are smaller compared to the fission sensitivity results over the same neutron energy ranges.

There is a small sensitivity peak to the system k_{eff} (~0.015) to small changes in ^{9}Be elastic scattering at fast neutron energies (> 1 MeV) that is consistent with the large beryllium reflector used in HFIR compared to the sensitivities at thermal energies. The sensitivity at larger neutron energies rather than at thermal energies indicates no significant sensitivity to the ^{9}Be-bound scattering kernel for beryllium metal.

The HFIR LEU fuel plates will contain 10 wt. % natural molybdenum in the U-Mo fuel meat , and the k_{eff} of the HFIR LEU core appears to be sensitive to small perturbations in the ^{95}Mo capture reaction (integral

sensitivity ~0.011), although the sensitivity is small compared to the other isotopes of interest ($\pm 10^{-2}$ to 10^{-4} range). The total integral sensitivity to the molybdenum isotopes for the capture reaction is also small (-0.0118) compared to the Be bound, hydrogen, and uranium isotopes.

Because of the large absorption cross section for ^{238}U, especially in the resonance region of the neutron spectrum, resonance self-shielding effects within ^{238}U in the LEU fuel during operations become rather significant. There are significant negative sensitivities of ^{238}U capture in the resonance region of the neutron energy spectrum and a small positive sensitivity peak for ^{238}U fission above 1 MeV. The integral sensitivity for ^{238}U capture and fission are ~0.08 and ~0.02, respectively. Even with the larger ^{238}U concentration in the LEU fuel, there is less sensitivity to ^{238}U perturbations than expected considering the ^{238}U concentration increases significantly with the HFIR core fuel modification from HEU (~93.2 wt. % ^{235}U) to LEU (~19.75 wt. % ^{235}U) fuel.

The DP calculation results for the isotopes and reactions of interest compare well with the CE TSUNAMI-3D results. The use of CE TSUNAMI-3D has made this type of calculation possible for complex geometrical configurations such as the HFIR LEU core configuration.

5. TSUNAMI-IP CALCULATIONS

5.1 INTERNATIONAL HANDBOOK OF EVALUATED CRITICALITY SAFETY BENCHMARK EXPERIMENTS

Calculation results from radiation transport codes such as KENO-VI need to be compared to experimental data to ensure that the computational methodology and nuclear data are providing adequate results. This is important because safety and design decisions are made based on radiation transport calculation results. An experimental database is provided for a variety of system parameters and operations of interest in the *International Handbook of Evaluated Criticality Safety Benchmark Experiments* (IHECSBE) [20]. The IHECSBE experimental database contains numerous evaluations for a variety of critical experimental configurations involving LEU, intermediate enriched uranium (IEU), and HEU for metal, solution, compound, and miscellaneous systems. The IHECSBE is part of the International Criticality Safety Benchmark Evaluation Project and is published annually. A wide variety of critical experimental benchmarks were chosen from IHECSBE for a similarity assessment and compared to the sensitivity results for the HFIR LEU CE TSUNAMI-3D model.

5.2 SIMILARITY ASSESSMENT

The sensitivity analysis performed for the HFIR LEU core yields a significant amount of information about the similarities and differences between fissionable material systems, including the HFIR LEU core and similar critical benchmark experiments. For code validation purposes, sensitivity results can be combined with nuclear data uncertainty information to determine whether or not two systems are similar enough to be used in code validation efforts. The sensitivity coefficients generated by CE TSUNAMI-3D represent the fractional change on the system k_{eff} due to a fractional change in nuclear data. The sensitivity data produced by CE TSUNAMI-3D are provided as energy-dependent sensitivity profiles and as integral sensitivities. The CE TSUNAMI-3D integrated sensitivities are not used in the similarity assessment. Uncertainty analysis is also performed by CE TSUNAMI-3D for the purpose of quantifying the energy-dependent uncertainty in k_{eff} due to the uncertainty in nuclear data. This analysis considers the propagation of estimated cross section uncertainty information to the calculated k_{eff} value of a given system using the sensitivity coefficients. The procedure also provides an energy-, nuclide-, and reaction-dependent comparison of two systems to yield an estimate of the correlated uncertainty between them. The correlated uncertainties can be represented by correlation coefficients, in this case c_k, which effectively represent the degree of correlation in the uncertainties between the two systems. The values of the correlation coefficient are valid over a range of $-1 \leq c_k \leq 1$, where $c_k = 0$ indicates no correlation, $c_k = 1$ indicates full correlation and $c_k = -1$ indicates full anti-correlation. Typically, the closer the correlation coefficient is to a value of unity, the better the correlation between two fissile systems. A value of c_k above 0.8–0.9 represents modest similarity between two systems, while a value of c_k above 0.9 indicates that the two systems are similar enough for the critical benchmark experiment to be applicable for use with validation efforts [20]. The correlation between two fissile material systems, in this case the HFIR LEU core and a benchmark critical experiment, could be related because they contain the same types of materials. Systems with the same materials and similar spectra would be correlated, while systems with different materials or spectra would not be correlated [21]. The underlying principle associated with use of the c_k parameter is that two systems with similar sensitivity to the same higher uncertainty nuclear data will have the same nuclear-data related bias. The c_k parameter is useful because it provides a single quantity relating the similarity between two systems considering both the sensitivity of the k_{eff} to small changes in material properties and propagated uncertainties in nuclear data.

5.3 TSUNAMI-IP RESULTS

The results of the TSUNAMI-IP comparison analysis that considered 750 critical benchmark experiments are illustrated in Fig. 24 and Fig. 25. There were no critical benchmark experiments identified with c_k values greater than 0.9; however, there was some similarity (not as much as desired, i.e., $c_k > 0.9$) between the HFIR LEU core model and critical benchmark experiments for verification and validation purposes.

Fig. 25 illustrates the 112 experiments with c_k values between 0.8 and 0.9, with the highest c_k value being 0.87. These 112 experiments and experimental series are listed in Table 3 sorted by c_k value. They are the points plotted in Fig. 26 with c_k values greater than 0.8. The top three experiments noted (car10, car07, and car08) were Rocky Flats experiments that were conducted in the late 1970s using cubes of LEU (< 10 wt. % enrichment) U_3O_8 damp powders [22]. Two other similar Rocky Flats experiments, car17 and car18, also have c_k values greater than 0.8. The "car" experiments are not currently included in the IHECSBE. A variety of other LEU critical benchmarks were also identified with c_k values greater than 0.8 (LEU-COMP-THERM experiment series 9, 10, 12, 17, 18, 20, 21, 22, 24, 25, 26, 32, 40, 79, and HEU-MET-THERM-006 and LEU-SOL-THERM-001 and -017). [20]

The results of this effort have identified some critical benchmarks of moderate applicability that can be used for validation efforts; however, the similarity between the HFIR LEU core model and the identified experiments is less than it should be for use in criticality validation studies. Without sufficiently applicable critical benchmark experiments to validate the computational method, the bias and bias uncertainty values used to derive an upper subcritical limit for subsequent criticality safety analysis should include additional margin to cover validation deficiencies and would thus tend to be larger than desired. One conclusion that can be drawn from this comparison analysis is the need for benchmark-quality critical experiments for an LEU HFIR core to support criticality safety and reactor physics calculations for core conversion activities. It would be desirable for these measurements to be performed in a facility such as the proposed LPCF at ORNL. The close proximity to the HFIR reactor facility would allow measurements of excess reactivity to be performed to verify manufacturing techniques in a manner similar fashion to those performed by the Y-12 critical experiment facility in the 1960s prior to the new cores being loaded into the pressure vessel.

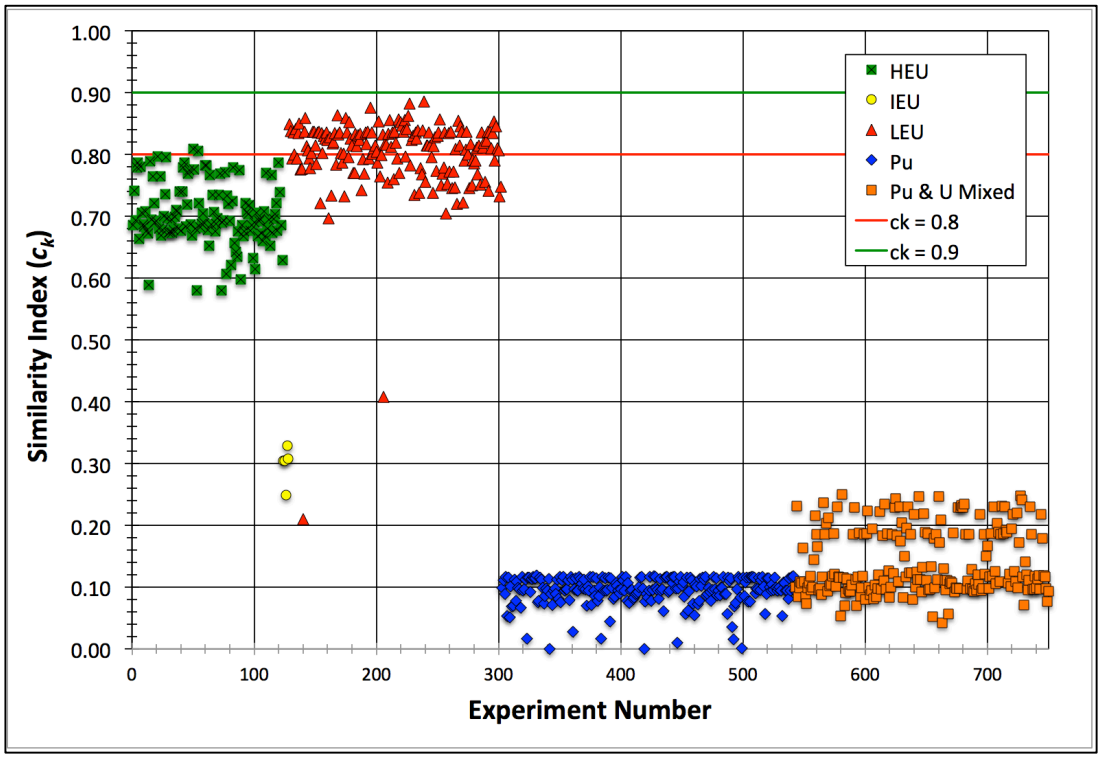

Fig. 25. Composite plot of TSUNAMI-IP comparison results for the HFIR LEU core model.

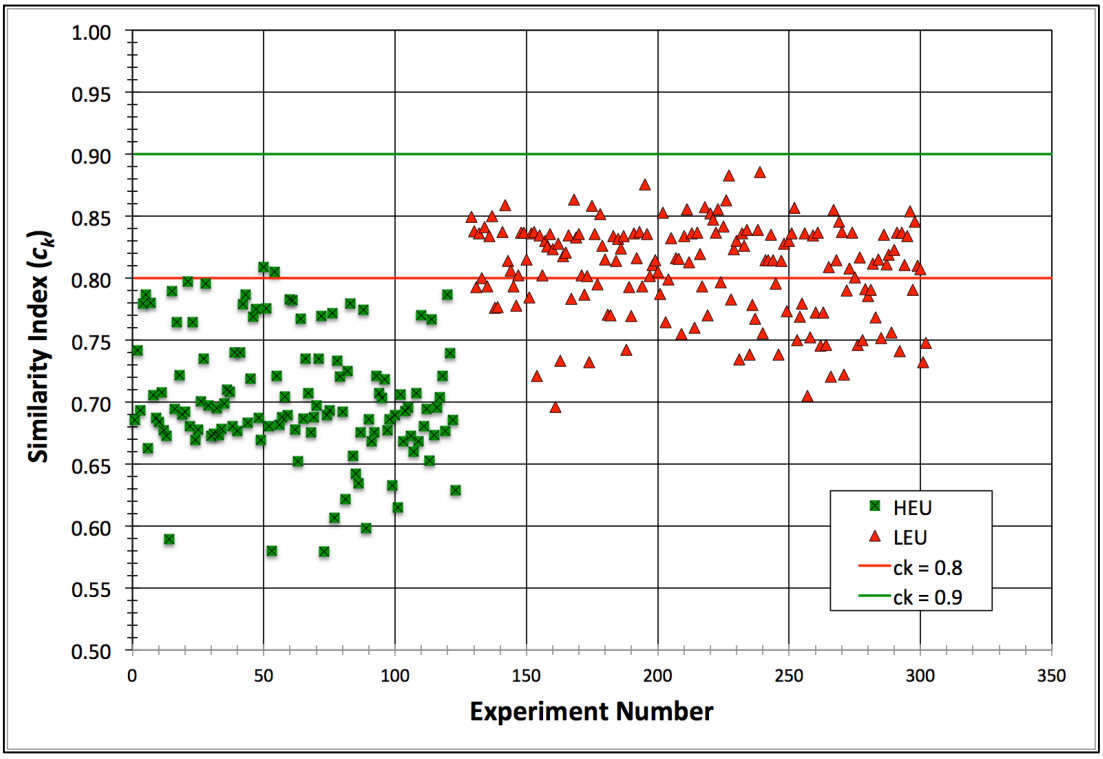

Fig. 26. TSUNAMI-IP comparison results with highest similarity index.

Table 3. Similarity index values for benchmark-critical experiments from TSUNAMI-IP analysis

Experiment number	Experiment series	c_k	σ	Experiment number	Experiment series	c_k	σ	Experiment number	Experiment series	c_k	σ
239	car10	0.8857	0.0007	256	lct009-23	0.8363	0.0007	288	lct079-6	0.8191	0.0006
227	car07	0.8828	0.0007	213	lct009-14	0.8363	0.0007				
195	car08	0.8756	0.0007	232	lct079-5	0.8362	0.0007	164	lct010-05	0.818	0.0009
168	lct010-16	0.8634	0.0013	191	lct040-02	0.8362	0.0007	277	lct26c4	0.8168	0.0007
226	car18	0.8628	0.0007	152	lct009-18	0.8362	0.0007	207	lct010-26	0.8164	0.0007
142	lct040-01	0.8588	0.0007	251	lct010-04	0.8361	0.0007	192	lct012-01	0.8164	0.0007
175	lct040-03	0.8587	0.0007	132	lct009-06	0.836	0.0007	208	lct010-25	0.8154	0.0007
218	lct010-19	0.8572	0.0007	196	lct009-13	0.8357	0.0007	180	lct012-02	0.8152	0.0007
252	lct32a3	0.8567	0.0007	159	lct009-03	0.8357	0.0007	150	lct012-03	0.815	0.0007
211	lct010-18	0.8557	0.0007	176	lct009-01	0.8355	0.0007	284	lct21c5	0.8149	0.0008
223	lct010-23	0.8554	0.0007	170	lct009-04	0.8354	0.0007	241	lct21c4	0.8147	0.0008
267	lct32a2	0.8551	0.0007	286	lct009-11	0.8353	0.0007	244	lct21c6	0.8144	0.0008
296	lct22c1	0.8541	0.0007	243	lct009-02	0.8353	0.0007	268	lct012-04	0.8144	0.0007
202	lct010-17	0.8531	0.0007	166	lct009-10	0.8348	0.0007	199	lct012-08	0.8144	0.0007
220	lct010-30	0.8523	0.0007	259	lct009-25	0.8347	0.0007	242	lct012-05	0.8143	0.0007
178	lct32a1	0.852	0.0007	155	lct21c1	0.8343	0.0007	247	lct012-07	0.8141	0.0007
137	lct010-28	0.8503	0.0007	295	lct21c3	0.8342	0.0007	143	lct012-06	0.8139	0.0007
129	lct010-29	0.8497	0.0007	136	lct009-27	0.8342	0.0007	184	lct010-11	0.8138	0.0007
221	car17	0.8474	0.0007	183	lct21c2	0.8341	0.0007	212	lct017-09	0.813	0.0007
269	lct010-22	0.8457	0.0007	187	lct009-26	0.834	0.0007	282	lct017-22	0.8117	0.0007
298	lct24c1	0.8455	0.0007	210	lct26c1	0.8338	0.0006	287	lct010-24	0.8112	0.0008
225	lct010-15	0.8418	0.0007	169	lct079-4	0.8327	0.0007	198	lct012-09	0.8107	0.0007
134	lct010-27	0.8414	0.0008	205	lct010-08	0.8321	0.0007	294	lct012-10	0.8104	0.0007
238	lct26c2	0.8389	0.0007	185	lct010-07	0.8317	0.0008	299	lct017-14	0.8103	0.0007
234	lct010-13	0.8388	0.0007	250	lct010-12	0.8303	0.0007	265	lct25c1	0.8092	0.0007
130	lct010-14	0.8377	0.0007	230	lct26c3	0.8302	0.0007	50	hmt006-23	0.8091	0.0007
153	lct009-07	0.8375	0.0007	157	lct079-3	0.8301	0.0006	273	lct017-21	0.8079	0.0007
141	lct009-20	0.8375	0.0007	248	lct079-1	0.828	0.0006	300	lct017-13	0.8075	0.0007
270	lct009-21	0.8372	0.0007	162	lct079-2	0.8276	0.0006	144	lct017-03	0.8064	0.0007
193	lct009-16	0.8371	0.0007	233	lct18c1	0.8263	0.0006	54	hmt006-22	0.8053	0.0007
291	lct009-17	0.837	0.0007	179	lct079-10	0.826	0.0007	200	lct017-20	0.8052	0.0007
293	lct009-09	0.8369	0.0007	158	lct010-21	0.8257	0.0007	171	lct20c1	0.8023	0.0007
274	lct009-19	0.8368	0.0007	186	lct22c2	0.8238	0.0006	147	lct017-12	0.8023	0.0007
149	lct009-24	0.8368	0.0007	229	lct079-9	0.8237	0.0007	156	lct017-25	0.8022	0.0007
148	lct009-05	0.8368	0.0007	160	lct010-06	0.8232	0.0008	173	lst01c1	0.8017	0.0006
222	lct009-22	0.8367	0.0007	290	lct079-8	0.8228	0.0007	197	lct017-08	0.8016	0.0007
215	lct009-08	0.8367	0.0007	165	lct010-20	0.8207	0.0007	275	lct010-10	0.8005	0.0007
261	lct009-15	0.8365	0.0007	216	lct079-7	0.8196	0.0006				

6. TSUNAMI-3D ANALYSIS OF FUEL ELEMENT MODELING ASSUMPTIONS

6.1 HOMOGENIZED FUEL ELEMENT ASSUMPTIONS

Previous HFIR reactor physics studies [1] have included modeling simplifications to reproduce the involute geometry of the inner and outer HFIR fuel elements. This simplification was achieved by homogenizing the fuel meat, the aluminum cladding, and the water moderator between the fuel plates for each of the fuel elements. These simplifications have provided reasonable results in numerous reactor physics studies performed for the HFIR HEU core because of the small concentration of ^{238}U in the HEU core which consists of ~93 wt. % ^{235}U and ~7 wt. % ^{238}U. The core model is arranged into axial and radial zones to closely represent the inner and outer fuel elements and the moderator configuration. The proposed LEU core will contain LEU consisting of 19.75 wt. % ^{235}U and 80.25 wt. % ^{238}U, with a larger concentration of ^{238}U compared to the HEU core. This results in more significant resonance self-shielding effects in the fuel. This effect tends to harden the neutron spectrum via epithermal neutron resonance absorption in the ^{238}U in LEU, which, in turn, results in reduced thermal utilization in the core and a lower system k_{eff}. The option to homogenize the fuel element constituents simplifies the geometric characteristics of the model significantly but could result in more neutron absorption via decreased self-shielding effects compared to the involute geometrical configuration. Neutron moderation in the water within the homogenized water/fuel mixture increases the chances of resonance absorption in the ^{238}U. Because of the self-shielding effects, it is possible that the homogeneous modeling assumption could misrepresent the actual core physics. Recent HFIR LEU core analyses [7, 8] consider the explicit representation of the HFIR involute fuel geometry using MCNP. Comparison results between homogeneous and explicit representations of the HFIR fuel plates are satisfactory with HEU fuel; however, the recent MCNP calculations indicate the homogenous fuel plate approximation results for LEU fuel does not compare as well with the explicit fuel plate approximation results [8]. The use of Whisper [9] with MCNP could allow for the comparison of the SCALE CE TSUNAMI-3D S/U analysis results with an independent code package. The infinite homogeneous and explicit slab models considered in 6.2 does provide insight into the effect of considering the homogeneous and explicit fuel approximations for the LEU HFIR fuel analyses.

6.2 HOMOGENEOUS AND SLAB TSUNAMI-3D CALCULATIONS

6.2.1 Description of the Homogeneous and Slab TSUNAMI-3D Models

Two simple CE TSUNAMI-3D calculations using the CLUTCH methodology, discussed previously, were generated to examine the sensitivity profiles of the HFIR LEU fuel constituents in two geometric configurations: an infinite homogeneous (mixture of plate fuel and moderator) configuration and an infinite lattice slab (straight fuel plates with interstitial water present) configuration. The infinite homogeneous model is a simple geometric configuration that considers the LEU fuel, cladding, and moderator (water) in a fuel plate mixed together in a simple volume-averaged homogeneous mixture. There are no spatial self-shielding effects in the homogeneous configuration, but resonance self-shielding effects as a result of ^{238}U and moderator mixture will be considered by the calculation. These effects may be represented by a slightly lower k_∞ for the homogeneous case than the heterogeneous model. The infinite slab cell model considers a slab lattice representation of a LEU fuel plate as described in Ref. 1, with mirror boundary conditions in the y- and z-directions and periodic boundary conditions in the x-direction. This approximates an infinite arrangement of fuel plate and moderator, and it also accounts for the spatial self-shielding effects. The actual HFIR LEU fuel is configured in an involute geometry that preserves the distance between fuel plates. The purposes of generating these two simple models is to compare the sensitivity profiles for the core constituents in the two geometric approximations and to examine whether there are potential issues related to homogenizing moderator, cladding, and fuel in the HFIR LEU core for reactor physics studies. The CE TSUNAMI-3D sensitivity results for the two

configurations will be compared. The material specifications for both the slab lattice and homogeneous models are provided in Table 4 and Table 5, respectively. The slab thicknesses for each material constituent of the fuel element is provided in the mixture column in Table 4.

Table 4. Slab model material specifications

Mixture	Density (g/cc)	Nuclide	Atom density (atoms/bn-cm)	Weight fraction (%)
1	0.98465	1001	6.58E-02	1.12E-01
(water – thickness = 0.0635 cm) [1]		8016	3.29E-02	8.88E-01
2	2.6971	1001	3.39E-04	2.10E-04
(aluminum clad – thickness = 0.0254 cm) [1]		6000	1.35E-03	1.00E-02
		13027	5.85E-02	9.73E-01
		14028	3.20E-04	5.52E-03
		14029	1.63E-05	2.90E-04
		14030	1.07E-05	1.98E-04
		22046	2.10E-06	5.95E-05
		22047	1.90E-06	5.48E-05
		22048	1.88E-05	5.54E-04
		22049	1.38E-06	4.15E-05
		22050	1.32E-06	4.06E-05
		24050	2.65E-06	8.15E-05
		24052	5.11E-05	1.63E-03
		24053	5.79E-06	1.89E-04
		24054	1.44E-06	4.79E-05
		25055	2.22E-05	7.51E-04
		26054	5.96E-06	1.98E-04
		26056	9.35E-05	3.22E-03
		26057	2.16E-06	7.57E-05
		26058	2.87E-07	1.03E-05
		28058	3.96E-06	1.41E-04
		28060	1.53E-06	5.63E-05
		28061	6.63E-08	2.49E-06
		28062	2.11E-07	8.06E-06
		28064	5.38E-08	2.12E-06
		29063	7.08E-05	2.74E-03
		29065	3.16E-05	1.26E-03
3	6.49	40090	2.20E-02	5.07E-01
(zirconium – thickness 0.0025 cm) [1]		40091	4.81E-03	1.12E-01
		40092	7.35E-03	1.73E-01
		40094	7.45E-03	1.79E-01
		40096	1.20E-03	2.94E-02
4	17.02	42092	1.58E-03	1.41E-02
(U[19.75] &		42094	9.86E-04	9.03E-03
Molybdenum – half thickness = 0.0291 cm) [1]		42095	1.70E-03	1.57E-02
		42096	1.78E-03	1.67E-02
		42097	1.02E-03	9.66E-03
		42098	2.58E-03	2.47E-02
		42100	1.03E-03	1.01E-02
		92234	6.50E-05	1.49E-03
		92235	7.75E-03	1.78E-01
		92236	3.55E-04	8.18E-03
		92238	3.07E-02	7.13E-01
5	2.71	13027	6.01E-02	9.93E-01
(aluminum – thickness = 0.0129 cm) [1]		14028	1.34E-04	2.30E-03
		14029	6.81E-06	1.21E-04
		14030	4.49E-06	8.25E-05
		25055	7.43E-06	2.50E-04
		26054	4.27E-06	1.41E-04
		26056	6.70E-05	2.30E-03
		26057	1.55E-06	5.40E-05
		26058	2.06E-07	7.31E-06
		29063	3.11E-05	1.20E-03
		29065	1.39E-05	5.52E-04

Table 5. Homogeneous model material specifications

Mixture	Density (g/cc)	Nuclide	Atom density (atoms/bn-cm)	Weight fraction (%)
1 (water, aluminum, zirconium, molybdenum and U[19.75])	5.1992	1001	3.30E-02	1.06E-02
		6000	2.71E-04	1.04E-03
		8016	1.65E-02	8.41E-02
		13027	1.48E-02	1.27E-01
		14028	7.09E-05	6.33E-04
		14029	3.60E-06	3.33E-05
		14030	2.38E-06	2.28E-05
		22046	4.20E-07	6.17E-06
		22047	3.79E-07	5.68E-06
		22048	3.76E-06	5.75E-05
		22049	2.76E-07	4.31E-06
		22050	2.64E-07	4.21E-06
		24050	5.30E-07	8.45E-06
		24052	1.02E-05	1.70E-04
		24053	1.16E-06	1.96E-05
		24054	2.88E-07	4.97E-06
		25055	4.83E-06	8.47E-05
		26054	1.41E-06	2.43E-05
		26056	2.21E-05	3.95E-04
		26057	5.11E-07	9.28E-06
		26058	6.79E-08	1.26E-06
		28058	7.92E-07	1.47E-05
		28060	3.05E-07	5.84E-06
		28061	1.33E-08	2.58E-07
		28062	4.23E-08	8.36E-07
		28064	1.08E-08	2.20E-07
		29063	1.57E-05	3.16E-04
		29065	7.02E-06	1.46E-04
		40090	4.41E-04	1.27E-02
		40091	9.61E-05	2.79E-03
		40092	1.47E-04	4.31E-03
		40094	1.49E-04	4.47E-03
		40096	2.40E-05	7.35E-04
		42092	3.62E-04	1.06E-02
		42094	2.26E-04	6.78E-03
		42095	3.89E-04	1.18E-02
		42096	4.08E-04	1.25E-02
		42097	2.34E-04	7.24E-03
		42098	5.92E-04	1.85E-02
		42100	2.37E-04	7.55E-03
		92234	1.49E-05	1.11E-03
		92235	1.78E-03	1.33E-01
		92236	8.14E-05	6.14E-03
		92238	7.03E-03	5.34E-01

6.2.2 Homogeneous and Slab Model Results

The results of the CE TSUNAMI-3D calculations are summarized in Table 6–Table 8. Table 6 and Table 7 provide the integral sensitivity results for the homogeneous fuel model and slab fuel model, respectively, and Table 8 provides a comparison of the CE TSUNAMI results shown in Table 6 and Table 7. The results summarize the total sensitivity for either the homogeneous or slab geometry configurations. ^{9}Be bound is not considered in these configurations because the beryllium reflector is not included in these calculations, which consider only the constituents of the fuel plates and water moderator. Sensitivity data for zirconium are not examined in the sensitivity results. The DP results for both homogeneous and slab fuel models compare well (<1% difference) with the CE-TSUNAMI results.

Table 6. Comparison of CE TSUNAMI and DP results for the homogeneous configuration

Isotope	CE TSUNAMI			DP			Results comparison		
	S^a	$\sigma_S{}^b$	$\%\sigma_S$	S^a	$\sigma_S{}^b$	$\%\sigma_S$	% difference[c]	standard deviation difference[d]	difference[e]
^{1}H	0.0984	8.72E-04	0.89	0.0982	4.51E-04	0.46	0.27	0.27	0.00026
Mo	-0.0281	6.94E-05	0.25	-0.0281	1.29E-04	0.46	-0.09	0.17	0.00002
^{235}U	0.0637	6.52E-05	0.10	0.0637	2.95E-04	0.46	-0.01	0.02	-0.00001
^{238}U	-0.1025	1.96E-04	0.19	-0.1028	4.70E-04	0.46	-0.30	0.61	0.00031

[a] S = energy integrated sensitivity results
[b] σ_S = standard deviation of the energy integrated sensitivity results
[c] % difference = $\frac{(S_{TSUNAMI\text{-}3D}-S_{DP})}{S_{DP}}*100\%$
[d] standard deviation difference = $\left|\frac{(S_{TSUNAMI\text{-}3D}-S_{DP})}{\sqrt{\sigma_{TSUNAMI\text{-}3D}{}^2+\sigma_{DP}{}^2}}\right|$
[e] difference = $S_{TSUNAMI\text{-}3D} - S_{DP}$

Table 7. Comparison of CE TSUNAMI and DP results for the explicit slab configuration

Isotope	TSUNAMI			DP			Results comparison		
	S^a	$\sigma_S{}^b$	$\%\sigma_S$	S^a	$\sigma_S{}^b$	$\%\sigma_S$	% difference[c]	standard deviation difference[d]	difference[e]
^{1}H	0.1105	9.07E-04	0.82	0.1097	5.00E-04	0.46	0.65	0.69	0.00072
Mo	-0.0270	7.16E-05	0.27	-0.0270	1.22E-04	0.45	-0.13	0.25	0.00003
^{235}U	0.0586	1.08E-04	0.18	0.0587	2.61E-04	0.45	-0.14	0.29	-0.00008
^{238}U	-0.0961	2.10E-04	0.22	-0.0965	4.30E-04	0.45	-0.34	0.69	0.00033

[a] S = energy integrated sensitivity results
[b] σ_S = standard deviation of the energy integrated sensitivity results
[c] % difference = $\frac{(S_{TSUNAMI\text{-}3D}-S_{DP})}{S_{DP}}*100\%$
[d] standard deviation difference = $\left|\frac{(S_{TSUNAMI\text{-}3D}-S_{DP})}{\sqrt{\sigma_{TSUNAMI\text{-}3D}{}^2+\sigma_{DP}{}^2}}\right|$
[e] difference = $S_{TSUNAMI\text{-}3D} - S_{DP}$

The comparison results between the homogeneous and slab fuel plate models indicate that the integral sensitivity results for ^{1}H is about 10.95% less for the homogeneous fuel plate configuration compared to the slab lattice configuration. This is likely due to the heterogeneous configuration in which fuel layers are separated by water rather than fuel constituents are homogeneously mixed with water. The integral sensitivity results for Mo (total), ^{235}U, and ^{238}U are ~4.1%, ~8.7%, and ~6.7% larger, respectively, for the homogeneous fuel plate configuration than for the heterogeneous slab fuel plate configuration.

Table 9 provides the energy-integrated sensitivities and standard deviations for both the homogeneous and explicit slab configurations. The sensitivity data in Table 9 summarizes the sensitivity data as a function of nuclide and reaction. The results in this table clearly show the homogeneous configuration having larger sensitivities for ^{235}U and ^{238}U elastic scatter, capture, and fission reactions than the explicit slab or heterogeneous configuration. This is the case for molybdenum as well. Conversely, the sensitivity results for ^{1}H elastic scatter and capture reactions for the heterogeneous configuration are larger than those for the homogeneous configuration.

Table 8. Comparison of CE TSUNAMI results for homogeneous and slab configurations

Isotope	Homogeneous fuel plate configuration			Slab lattice configuration			% Difference[c]
	S^a	$\sigma_S{}^b$	$\%\sigma_S$	S^a	$\sigma_S{}^b$	$\%\sigma_S$	
^{1}H	0.0984	8.72E-04	0.89	0.1105	9.07E-04	0.82	-10.95
Mo	-0.0281	6.94E-05	0.25	-0.027	7.16E-05	0.27	4.07
^{235}U	0.0637	6.52E-05	0.1	0.0586	1.08E-04	0.18	8.70
^{238}U	-0.1025	1.96E-04	0.19	-0.0961	2.10E-04	0.22	6.66

[a] S = energy integrated sensitivity results
[b] σ_S = standard deviation of the energy integrated sensitivity results
[c] % difference = (Homogeneous- slab)*100%/(slab). A positive difference indicates that the isotope sensitivity in the slab configuration is less than the homogeneous configuration.

Table 9. Energy-integrated sensitivities and standard deviations for the homogeneous and explicit slab configuration

Isotope	Reaction	Direct perturbation		CE TSUNAMI-3D	
		S^a	$\sigma_S{}^b$	S^a	$\sigma_S{}^b$
Homogeneous Configuration					
^{1}H	Total	9.820E-02	4.510E-04	9.844E-02	8.720E-04
	Elastic Scatter			1.055E-01	8.724E-04
	Capture			-7.053E-03	8.196E-07
^{235}U	Total	6.370E-02	2.950E-04	6.370E-02	6.524E-05
	Elastic Scatter			-4.199E-04	5.378E-05
	Capture			-2.059E-01	2.047E-05
	Fission			2.711E-01	3.331E-05
	n,n'			-1.197E-03	2.007E-05
^{238}U	Total	-1.028E-01	4.70E-04	-1.025E-01	1.960E-04
	Elastic Scatter			9.903E-03	1.752E-04
	Capture			-1.293E-01	1.584E-05
	Fission			2.171E-02	2.082E-05
	n,n'			-6.149E-03	4.937E-05
Mo	Capture	-2.810E-02	1.290E-04	-2.810E-02	6.940E-05
$^{95}Mo^c$	Capture	NC[d]	NC	-1.582E-02	3.988E-06
Explicit Cell Configuration					
^{1}H	Total	1.105E-01	9.070E-04	1.105E-01	9.069E-04
	Elastic Scatter			1.184E-01	9.074E-04
	Capture			-7.924E-03	1.041E-06
^{235}U	Total	5.860E-02	1.080E-04	5.861E-02	1.0757E-04
	Elastic Scatter			-4.614E-04	5.541E-05
	Capture			-2.040E-01	2.319E-05
	Fission			2.641E-01	6.365E-05
	n,n'			-1.160E-03	4.321E-05
^{238}U	Total	-9.610E-01	2.100E-04	-9.612E-02	2.095E-04
	Elastic Scatter			8.809E-03	1.773E-04
	Capture			-1.213E-01	1.651E-05
	Fission			2.101E-02	2.110E-05
	n,n'			-5.953E-03	6.310E-05
Mo	Capture	-2.700E-02	1.220E-04	-2.700E-02	7.160E-05
$^{95}Mo^c$	Capture	NC[d]	NC[d]	-1.505E-02	4.006E-06

[a] S = energy integrated sensitivity results
[b] σ_S = standard deviation of the energy integrated sensitivity results
[c] The integral sensitivities for ^{92}Mo, ^{94}Mo, ^{96}Mo, ^{97}Mo, ^{98}Mo, and ^{100}Mo capture are small compared to ^{95}Mo capture sensitivity results and are not provided here but are provided in the energy-dependent sensitivity profiles in Fig. 18. The results for ^{X}Mo inelastic scattering sensitivity results are also very small (~10^{-4}) and are not provided here but are provided in Fig. 17.
[d] Not calculated

Fig. 27 and Fig. 28 illustrate the energy-dependent sensitivity profiles for ^{235}U total and ^{235}U fission and capture, respectively, for both configurations, homogeneous and slab lattice, on the same plot for comparison. Generally, for ^{235}U total, the slab configuration has sensitivity peaks with greater magnitude than the homogeneous configuration for thermal neutrons. For a neutron energy greater than ~1 eV, the homogeneous fuel configuration sensitivity peaks are slightly larger in value than the magnitude of the sensitivity peaks with the slab cell fuel configuration. For ^{235}U fission and capture, there is no significant sensitivity difference between the two fuel models, although there are some modest differences. Fig. 28 indicates higher sensitivity values (absolute value) below 1 eV for the slab configuration for ^{235}U fission and capture. Above ~1 eV, the homogeneous configuration results in slightly larger sensitivity magnitude than for the slab fuel model.

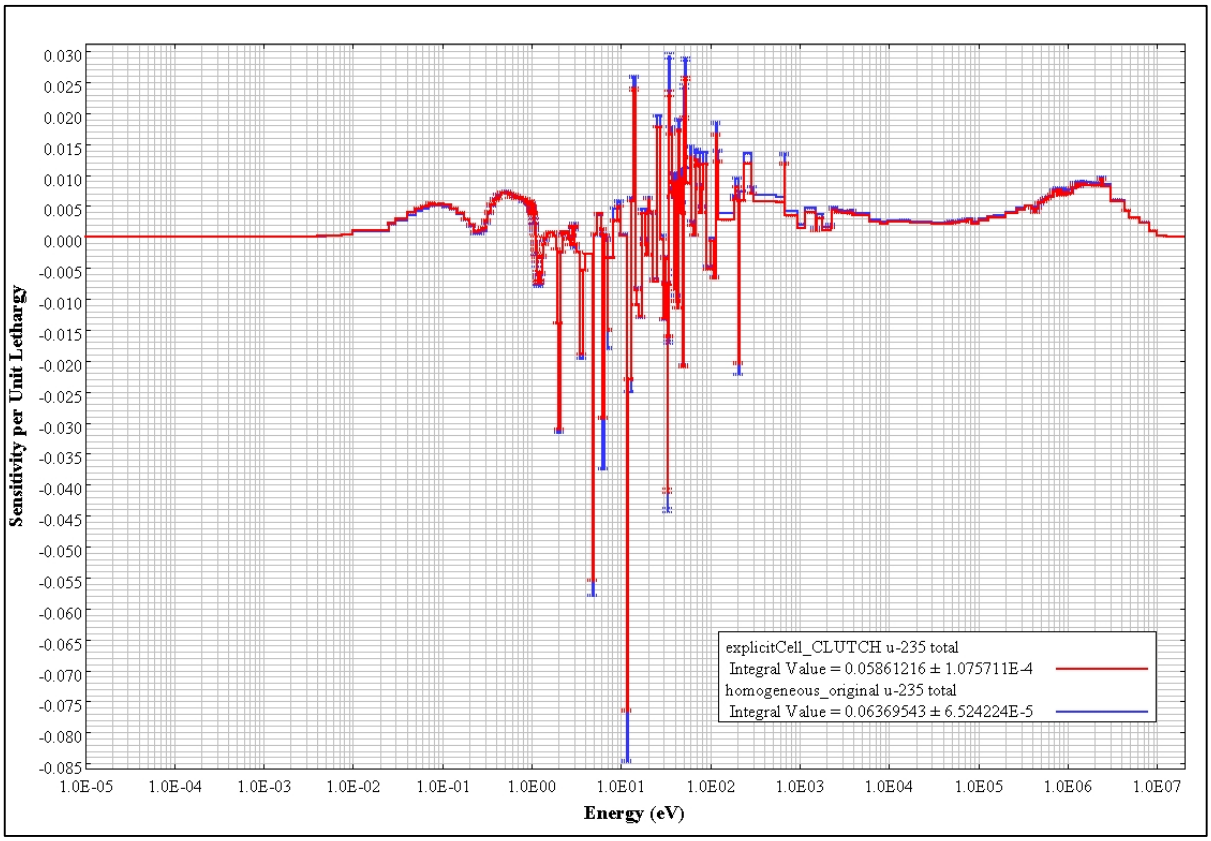

Fig. 27. Energy-dependent sensitivity profiles for ^{235}U (total) for the slab and homogeneous LEU fuel plate configurations.

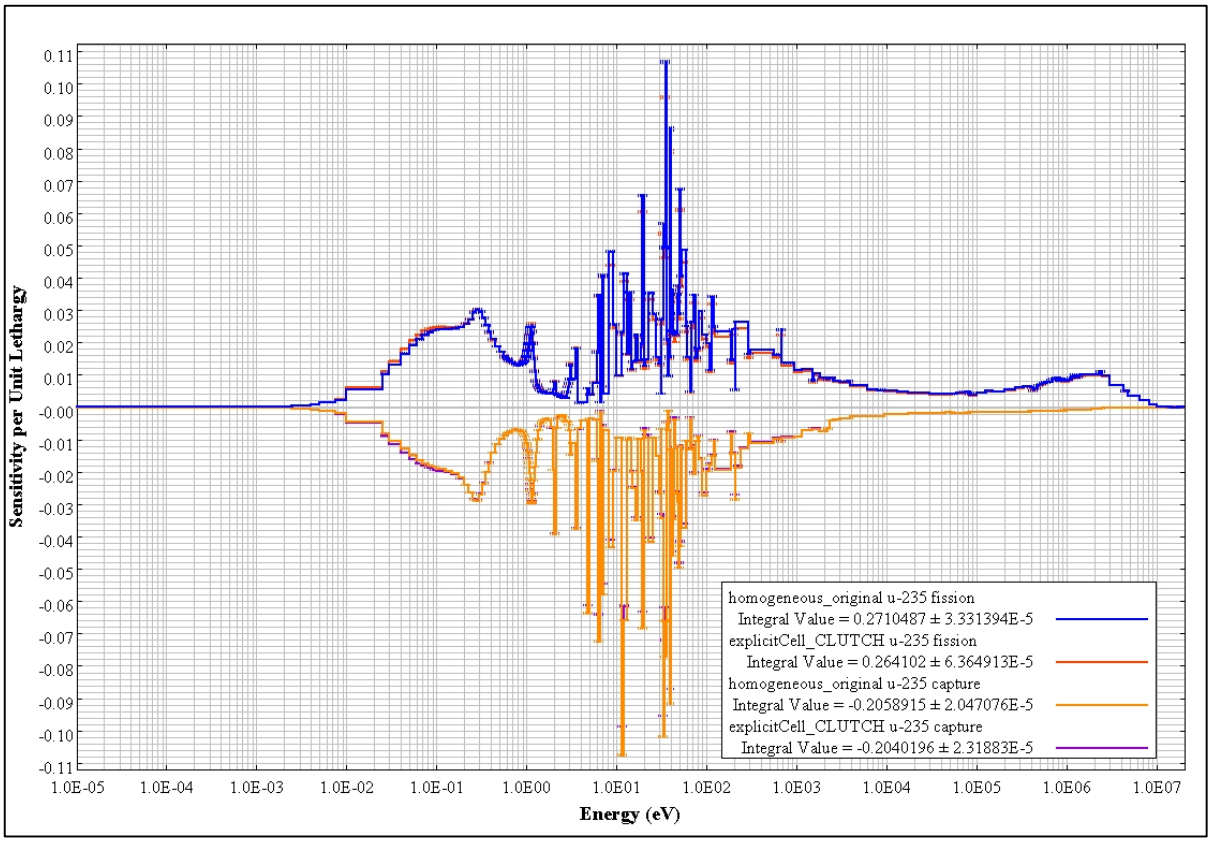

Fig. 28. Energy-dependent sensitivity profiles for ^{235}U (fission and capture) for the slab and homogeneous LEU fuel plate configurations.

Fig. 30 provides the energy-dependent sensitivity profiles for both fuel models for ^{238}U total. In the resonance region, the negative sensitivity results for the homogeneous fuel case are larger in magnitude than for the slab fuel configuration. The integral sensitivity is slightly larger in magnitude for the homogeneous fuel configuration than for the explicit fuel configuration.

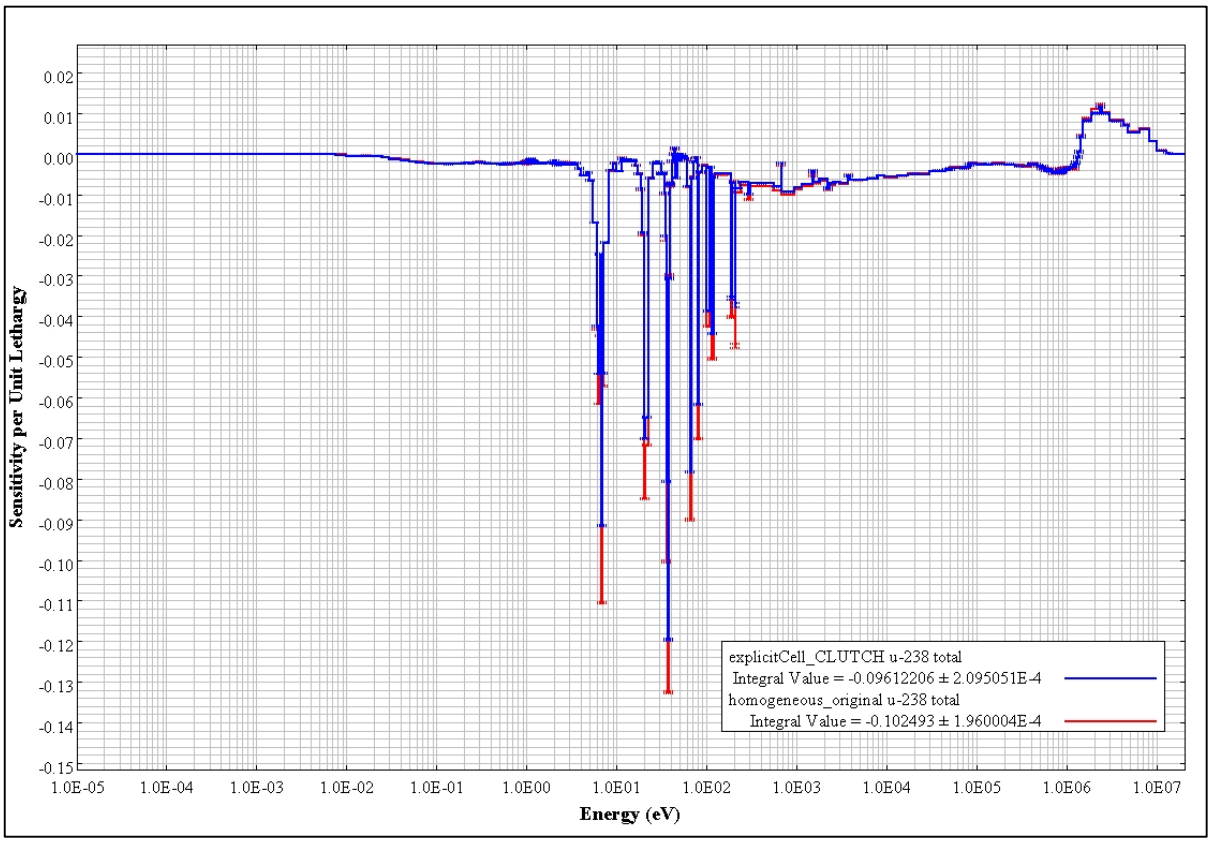

Fig. 29. Energy-dependent sensitivity profiles for ^{238}U (Total) for the slab and homogeneous LEU fuel plate configurations.

Fig. 30 indicates that there are some very small differences with the ^{238}U capture sensitivity in the resonance region with the homogeneous fuel model. These differences result in a slightly larger negative sensitivity than shown in the slab fuel model.

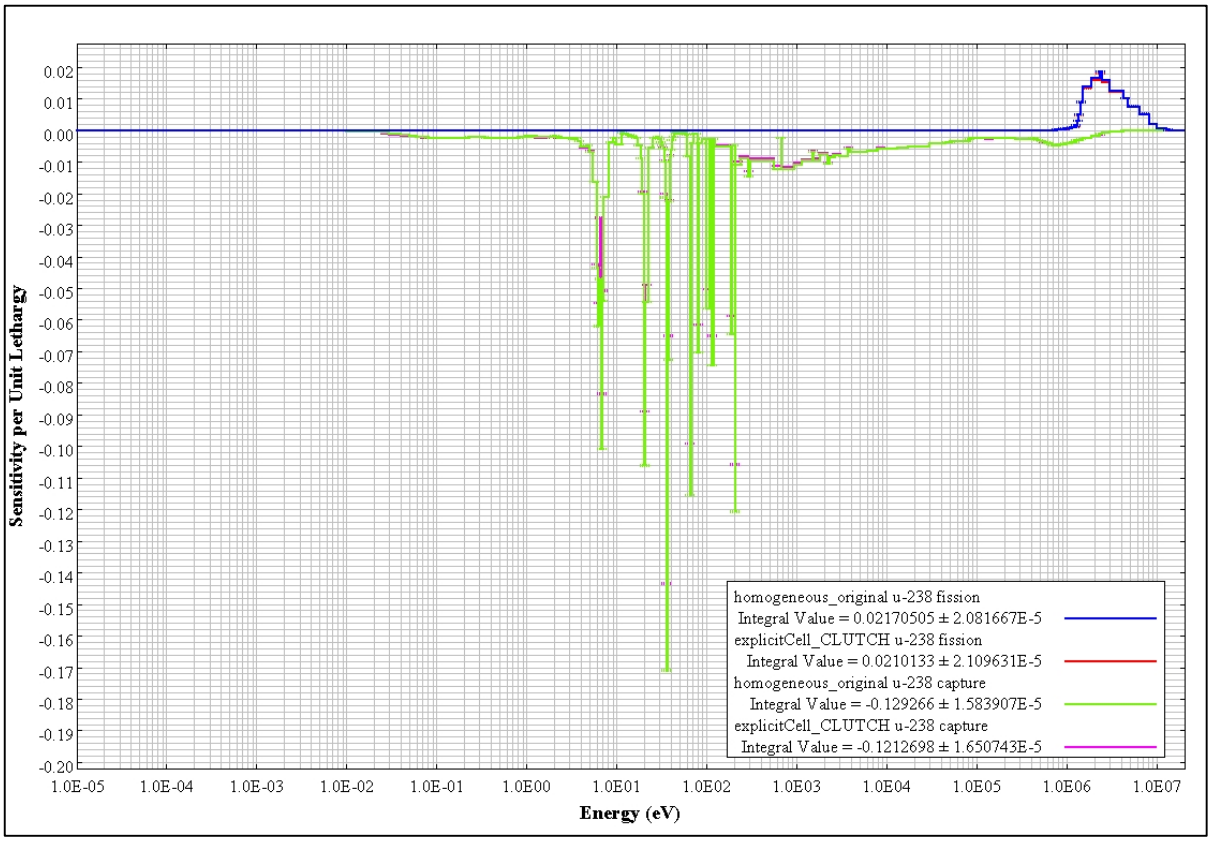

Fig. 30. Energy-dependent sensitivity profiles for ^{238}U (fission and capture) for the slab and homogeneous LEU fuel plate configurations.

Fig. 31 shows the energy-dependent sensitivity profiles for ^{235}U and ^{238}U elastic scattering and indicates that there is little difference between the two profiles, except for some small differences in the resonance region, showing a similar sensitivity for elastic scattering with the fissionable material regardless of the fuel plate model.

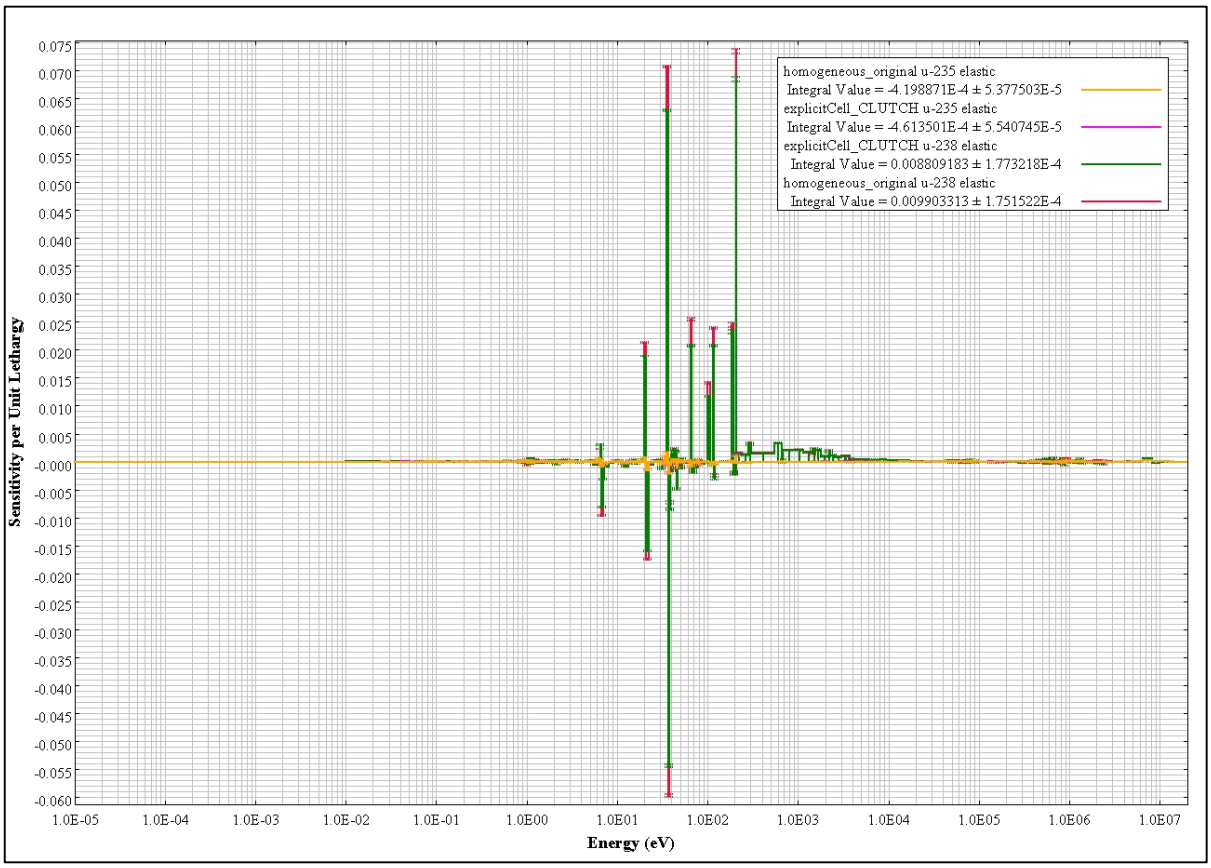

Fig. 31. Energy-dependent sensitivity profile for ^{235}U and ^{238}U (elastic scattering) for the slab and homogeneous LEU fuel plate configurations.

Fig. 32 shows the sensitivity profile results for the two fuel configurations for ^{1}H capture. Below neutron energies of 10 eV, the magnitudes of the sensitivity peaks are larger for the slab configuration than for the homogeneous configuration, as indicated by the difference in the two negative sensitivity peaks at ~0.1 and ~0.5 eV. Above neutron energies of greater than 10 eV, there are essentially no differences noted in the sensitivity profiles.

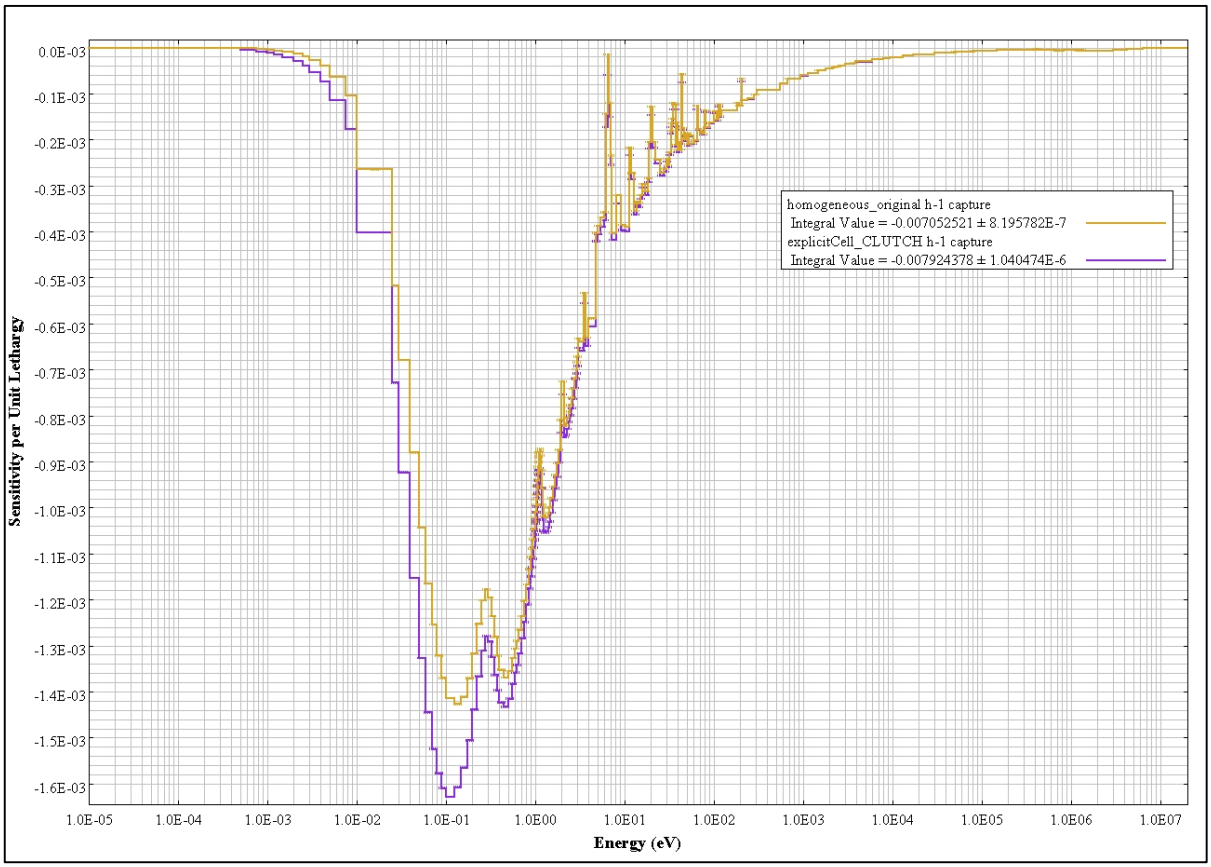

Fig. 32. Energy-dependent sensitivity profile for ^{1}H (Capture) for the slab and homogeneous LEU fuel plate configurations.

Fig. 33 shows the sensitivity profile results for ^{1}H elastic scattering. At thermal neutron and fast neutron energies, there are no discernable sensitivity differences between the slab and homogeneous fuel plate configurations. However, in the resonance region for neutron energies up to about 1 keV, some of the sensitivity peaks show a small difference in the sensitivity between the two models, and the slab fuel plate model shows a slightly larger sensitivity. The integral sensitivity for the slab fuel plate configuration is also slightly larger than for the homogeneous configuration.

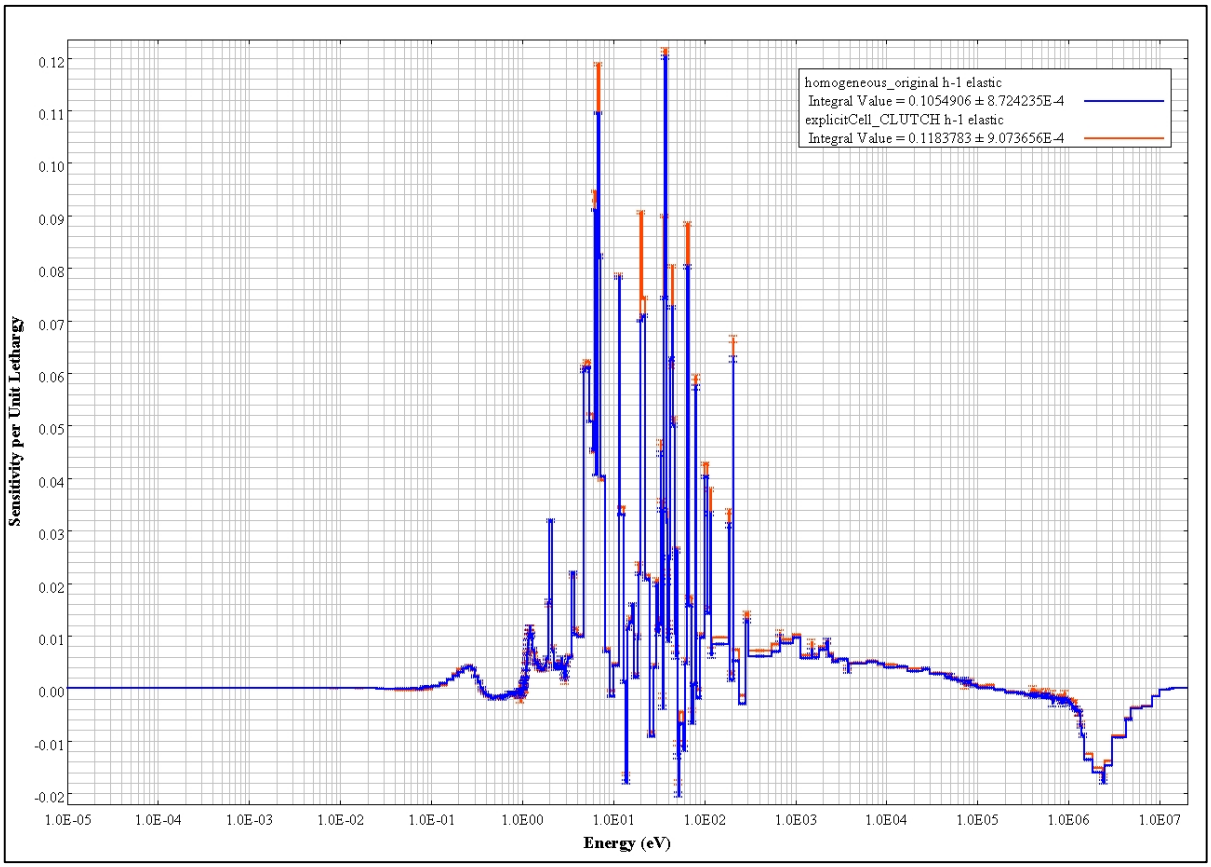

Fig. 33. Energy-dependent sensitivity profile for ^{1}H (elastic scattering) for the slab and homogeneous LEU fuel plate configurations.

Fig. 34 shows the energy-dependent sensitivity profile for ^{95}Mo, ^{96}Mo, and ^{98}Mo capture for the slab and homogeneous LEU fuel plate configurations. These results indicate some minor sensitivity differences between the two fuel model types. For ^{95}Mo, there is a significant negative sensitivity peak at about 45 eV. This peak indicates a greater negative sensitivity for the homogeneous model than for the slab model, probably due to the use of a homogeneous fuel arrangement rather than a heterogeneous fuel arrangement.

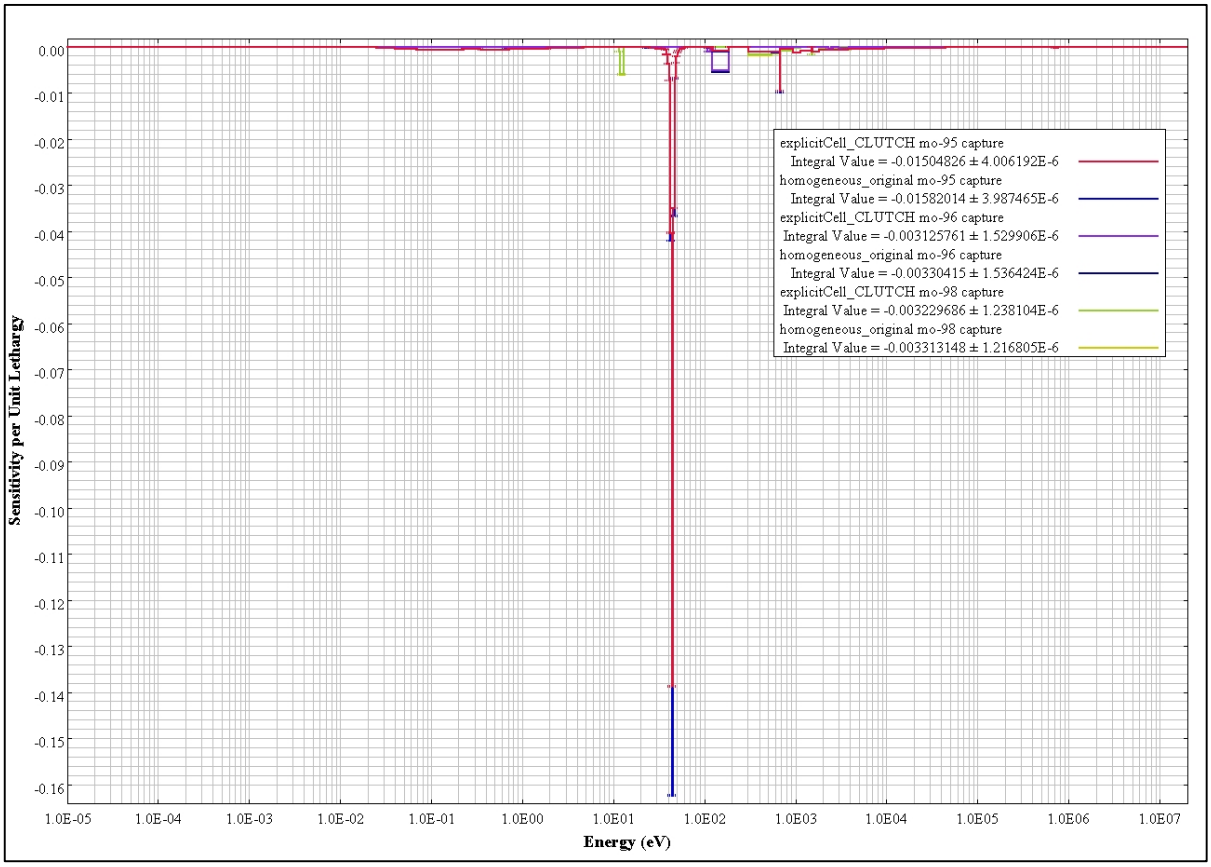

Fig. 34. Energy-dependent sensitivity profile for ^{95}Mo, ^{96}Mo, and ^{98}Mo (capture) for the slab and homogeneous LEU fuel plate configurations.

Fig. 35 shows the energy-dependent sensitivity profile for ^{95}Mo, ^{96}Mo, and ^{98}Mo elastic scattering for the slab and homogeneous LEU fuel plate configurations. There are no significant sensitivity differences noted for the molybdenum isotopes considered for elastic scattering.

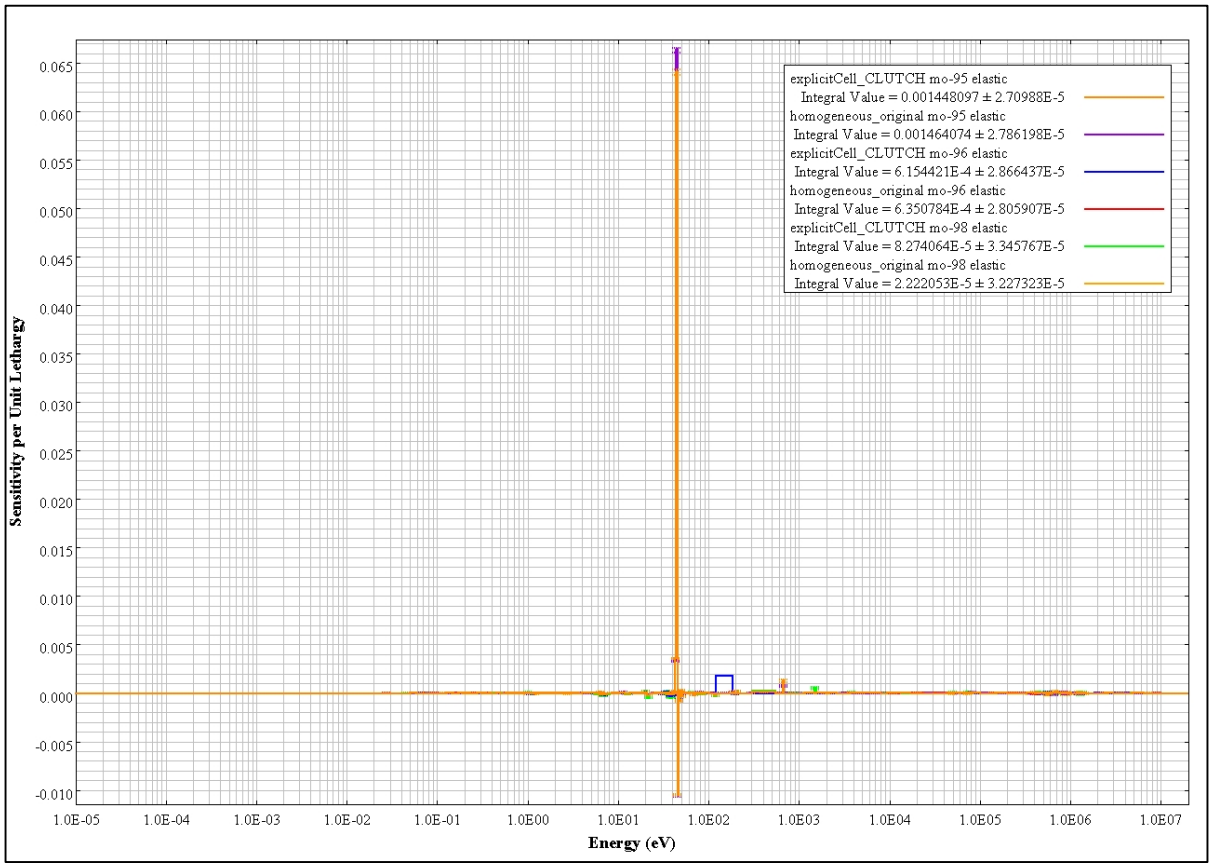

Fig. 35. Energy-dependent sensitivity profile for ^{95}Mo, ^{96}Mo, and ^{98}Mo (elastic scattering) for the slab and homogeneous LEU fuel plate configurations.

For a homogeneous system that considers fuel, cladding, and moderator as an infinite mixture the results suggest that the k_{eff} is more sensitive to small cross section perturbations than an slab cell system. This is likely due to the geometrical differences between homogeneous and slab (heterogeneous) configurations that have a significant impact to the system reactivity and neutron spectrum. For example, heterogeneous LEU systems will typically be more reactive than comparable homogeneous systems because of the reduction of neutron self-shielding within the fuel. For the two considered configurations, the heterogeneous slab cell configuration has a larger k_∞ (1.460804 ± 0.000047) than the homogeneous configuration (1.431629 ± 0.000053). In an infinite system, this indicates that there is more parasitic neutron absorption in the homogeneous case than in the slab cell case due to increase in self-shielding.

These calculations also did not consider effects from the adjacent control element materials, target materials, or beryllium reflector. This analysis could be expanded significantly if the models considered effects of these HFIR components and if the HFIR involute plate geometry were explicitly considered, although the slab cell configuration examines an approximate configuration of the fuel materials. Additional S/U calculations for a HFIR LEU core with the involute geometry explicitly modeled could be valuable for verifying these results and ensuring that self-shielding effects due to the increased quantity of

^{238}U do not impact future reactor physics studies related to the HFIR LEU core conversion project. Because of the differences noted between the two fuel configurations considered in this analysis, there appears to be a need for integral experiments to be performed to verify design attributes for the HFIR LEU core match up to performance expectations and to assist with computer code and nuclear data validation efforts. This approach would be similar to the HFIR design approach used in the 1960s.

7. CONCLUSION

The objective of this work has been to perform S/U analyses to investigate the quantitative need for benchmark-quality integral experiments for the validation of computational methods used to support the conversion of HFIR from HEU to LEU fuel. The calculation results of this work indicate a lack of applicable benchmark experiments for validating HFIR calculational methods to support LEU fuel conversion efforts.

The CE TSUNAMI-3D calculations have also been useful to determine those nuclide cross section sensitivities and uncertainties that can affect the system k_{eff} for a HFIR LEU core model. The results of the sensitivity/uncertainty analysis show the largest sensitivities with ^{1}H elastic scattering and ^{235}U fission cross sections, 0.269 and 0.304, respectively. There is also a significant positive sensitivity of the system k_{eff} to ^{235}U fission at thermal (~0.1 eV) energies (~0.062), indicating that the HFIR LEU core is sensitive to small changes in the content of ^{235}U in the core of the reactor, which is not unexpected. There is a small sensitivity of the system k_{eff} to small changes in ^{9}Be elastic scattering (~0.015) that is consistent with the use of a large beryllium reflector at HFIR. The HFIR LEU fuel plates contain an uranium-molybdenum fuel with 10 wt. % natural molybdenum; the k_{eff} of the HFIR LEU core appears to be sensitive to small perturbations in the ^{95}Mo and $^{96, 98}$Mo capture reaction, although the sensitivities are relatively small, ~10^{-2} to 10^{-4}, depending on the reaction, as shown in Fig. 15-Fig. 19. There is less sensitivity to ^{238}U nuclear data perturbations than expected considering that the ^{238}U concentration increases significantly in the HFIR LEU (~80 wt. % ^{238}U/U) compared to HEU (~ 7 wt. % ^{238}U/U) fuel. The ^{238}U sensitivity results indicate a small sensitivity in ^{238}U capture (approximately -0.12) with neutron energies in the resonance energy range. The direct perturbation calculations compared well with the CE TSUNAMI-3D results overall.

The LEU HFIR model results presented here were generated with the new CLUTCH methodology in TSUNAMI-3D and CE cross sections. Multigroup TSUNAMI-3D could not be successfully applied to the complex HFIR LEU model. The new CE TSUNAMI-3D sequence of SCALE has made it possible to successfully perform sensitivity analyses for complex geometrical configurations such as the HFIR LEU core.

The TSUNAMI-IP utility was used to determine applicable benchmark critical experiments for use in validation efforts. The c_k values generated by TSUNAMI-IP are used as an index for similarity assessment, and they represent the correlation of k_{eff} uncertainties between two models. This index quantifies the amount of shared uncertainty in the k_{eff} values of an application and a benchmark critical experiment due to uncertainties in the cross sections. A c_k value of 1.0 indicates that the uncertainties for the model and the critical benchmark experiment are from the same neutron cross sections and that the reactions are at the same energy, while a c_k value of 0.0 indicates that the uncertainties are completely unrelated. Typically, a c_k value of 0.9 or larger indicates good shared uncertainty between the model and benchmark experiment. The results in this work show that none of the nearly 750 critical benchmark experiments examined had a c_k index greater than 0.9, and 112 experiments with a c_k value between 0.8 and 0.9 indicate some moderate similarity with the HFIR LEU core model. One conclusion that can be drawn from this comparison analysis is the need for benchmark-quality critical experiments for an LEU HFIR core to support criticality safety and reactor physics calculations for core conversion activities. It would be desirable for these measurements to be performed in a facility such as the proposed LPCF at ORNL. The close proximity to the HFIR reactor facility would allow measurements of excess reactivity to be performed to verify manufacturing techniques in a manner similar fashion to those performed by the Y-12 critical experiment facility in the 1960s prior to the new cores being loaded into the pressure vessel. Results presented herein indicate that it will be important to consider validation tailored to both

heterogeneous (i.e., including explicit modeling of fuel, cladding, and moderator) and homogenous models that may be used to support the HFIR LEU core conversion.

Simple homogeneous (mixture of fuel, clad, and moderator) and heterogeneous slab (flat fuel plate) models of HFIR fuel plates in CE TSUNAMI-3D were generated to explore the effects of different fuel plate geometry approximations. A homogeneous arrangement of fuel, clad, and moderator could increase resonance self-shielding in the fuel plate. This is indicated by a larger k_∞ result for the heterogeneous configuration compared to that for the homogeneous configuration. In general, the results of these calculations show larger k_{eff} integral sensitivities to small cross section changes in molybdenum isotopes, ^{235}U, and ^{238}U for the homogeneous rather than for the heterogeneous fuel plate configuration, with differences of 4.07%, 8.70%, and 6.66%, respectively. The exception was ^{1}H, which had a total integral sensitivity which was 10.95% larger for the explicit slab configuration than for the homogeneous configuration. Recent HFIR LEU core analyses [7, 8] consider the explicit representation of the HFIR involute fuel geometry using MCNP. Comparison results between homogeneous and explicit representations of the HFIR fuel plates are satisfactory with HEU fuel with respect to eigenvalue and cycle lengths; however, for LEU fuel the explicit fuel plate approximation result in much larger cycle length. The use of Whisper [9] with MCNP will allow for the comparison of the SCALE CE TSUNAMI-3D S/U analysis results with an independent code package.

Future work may involve (1) using the HFIR LEU model with the IFP methodology available in CE TSUNAMI-3D, (2) using the HFIR HEU model to compare to HFIR LEU model CE TSUNAMI-3D results presented here, and (3) performing S/U calculations using the Whisper methodology in MCNP to compare to the results of the CE TSUNAMI-3D results in this report.

REFERENCES

1. G. Ilas and R. T. Primm III, *Low Enriched Uranium Fuel Design with Two-Dimensional Grading for the High Flux Isotope Reactor*, ORNL/TM-2010/318, Oak Ridge National Laboratory (April 2011).

2. *SCALE: A Comprehensive Modeling and Simulation Suite for Nuclear Safety Analysis and Design*, ORNL/TM-2005/39, Version 6.1, Oak Ridge National Laboratory, Oak Ridge, Tennessee, June 2011. Available from Radiation Safety Information Computational Center at Oak Ridge National Laboratory as CCC-785.

3. B. T. Rearden, *TSUNAMI-3D: Control Module for Three-Dimensional Cross-Section Sensitivity and Uncertainty Analysis for Criticality*, ORNL/TM-2005/39, Version 6.1, Sect. C9 (June 2011).

4. C. M. Perfetti and B. T. Rearden, "Continuous-Energy Eigenvalue Sensitivity Coefficient Calculations in TSUNAMI-3D," International Conference on Mathematics and Computational Methods Applied to Nuclear Science and Engineering, Sun Valley, Idaho, May 2013.

5. D. Ilas, *Development of a SCALE Model for High Flux Isotope Reactor Cycle 400*, Oak Ridge National Laboratory, ORNL/TM-2011/367, Oak Ridge National Laboratory, Oak Ridge, TN (February 2012).

6. D. F. Hollenbach, L. M. Petrie, S. Goluoglu, N. F. Landers, and M. E. Dunn, *KENO-VI: A General Quadratic Version of the KENO Program*, ORNL/TM-2005/39, Version 6.1, Sect. F17, Oak Ridge National Laboratory (June 2011).

7. G. Ilas, D. Chandler, B. Ade, E. Sunny, B. Betzler, and D. Pinkston, *Modeling and Simulations for the High Flux Isotope Reactor Cycle 400*, Oak Ridge National Laboratory, ORNL/TM-2015/36, March 2015.

8. B. Betzler, B. Ade, D. Chandler, G. Ilas, and E. Sunny "Optimization of Depletion Modeling and Simulation for the High Flux Isotope Reactor," ANS MC2015 Joint International Conference on Mathematics and Computation, Supercomputing in Nuclear Applications and the Monte Carlo Method, April 19-23, 2015.

9. B. C. Kiedrowski, et al., "Whisper: Sensitivity/Uncertainty-Based Computational Methods and Software for Determining Baseline Upper Subcritical Limits," *Nuc. Sci. Eng*., 181, p. 1-31, 2015.

10. R. D. Cheverton and T. M. Sims, *HFIR Core Nuclear Design," Oak Ridge National Laboratory*, ORNL-4621 (July 1971).

11. R. T. Primm III, R. J. Ellis, J. C. Gehin, D. L. Moses, J. L. Binder, and N. Xoubi, *Assumptions and Criteria for Performing a Feasibility Study of the Conversion of the High Flux Isotope Reactor Core to Use Low-Enriched Uranium Fuel*, ORNL/TM-2005/269, Oak Ridge National Laboratory (2006).

12. D. Renfro, D. Chandler, D. Cook, G. Ilas, P. Jain, and J. Valentine, "Preliminary Evaluation of Alternate Designs for HFIR Low-Enriched Uranium Fuel," Oak Ridge national Laboratory, ORNL/TM-2014/154, October 30, 2014.

13. E. C. Woolstenhulme, R. G. Damiana, K. A. Schreck, and A. M. Phillips, *Neutron Radiography Reactor Reactivity - Focused Lessons Learned*, Idaho National Laboratory, Idaho Falls, ID (November 2010).

14. B. T. Rearden and M. A. Jessee, *TSUNAMI Utility Modules*, ORNL/TM-2005/39, Version 6.1, Sect. M18, Oak Ridge National Laboratory (June 2011).

15. D. E. Mueller, B. T. Rearden, and D. F. Hollenbach, *Application of the SCALE TSUNAMI Tools for the Validation of the Criticality Safety Calculations Involving* ^{233}U, ORNL/TM-2008/196, Oak Ridge National Laboratory (January 2009).

16. C. M. Perfetti, *Advanced Monte Carlo Methods for Eigenvalue Sensitivity Coefficient Calculations*, doctoral dissertation, University of Michigan (2012).

17. M. L. Williams, D. Wiarda, K. S. Kim, M. E. Dunn and B. T. Rearden, "SCALE 6.2 Beta 4 Manual, Ch. 11 SCALE Cross-Section Libraries," Oak Ridge National Laboratory, 2015.

18. D. E. Mueller and B. T. Rearden, "Sensitivity Coefficient Generation for a Burnup Credit Cask Model Using TSUNAMI-3D," presented at the 2005 NCSD Topical Meeting, Knoxville, TN (September 19–22, 2005).

19. B. T. Rearden, "Perturbation Theory Eigenvalue Sensitivity Analysis with Monte Carlo Techniques," *Nucl. Sci. and Engr.*, **146**, 367-382 (2004).

20. *International Handbook of Evaluated Criticality Safety Benchmark Experiments*, NEA/NSC/DOC(95)03, NEA Nuclear Science Committee (September 2013).

21. B. L. Broadhead, B. T. Rearden, and C. M. Hopper, "Sensitivity- and Uncertainty-Based Criticality Safety Validation Techniques," *Nucl. Sci. Eng.* 146, 340–366 (2004).

22. G. Tuck and I. Oh, *Benchmark Critical Experiments on Low-Enriched Uranium Oxide Systems with H/U=0.77*, Rocky Flats Plant Report RFP-2895, NUREG/CR-0674, US Nuclear Regulatory Commission, Rockwell International Energy Systems Group, August 1979.